HHS Public Access

Author manuscript

Cell Rep. Author manuscript; available in PMC 2024 April 17.

Published in final edited form as:

Cell Rep. 2024 February 27; 43(2): 113722. doi:10.1016/j.celrep.2024.113722.

TRPM2 enhances ischemic excitotoxicity by associating with PKCγ

Pengyu Zong[1,2], **Jianlin Feng**[1], **Nicholas Legere**[3,4], **Yunfeng Li**[5], **Zhichao Yue**[1], **Cindy X. Li**[1,2], **Yasuo Mori**[6], **Barbara Miller**[7], **Bing Hao**[5], **Lixia Yue**[1,8,*]

[1]Department of Cell Biology, Calhoun Cardiology Center, University of Connecticut School of Medicine (UConn Health), Farmington, CT 06030, USA

[2]Institute for the Brain and Cognitive Sciences, University of Connecticut, 337 Mansfield Road, Unit 1272, Storrs, CT 06269, USA

[3]The Jackson Laboratory for Genomic Medicine, Farmington, CT, USA

[4]Department of Genetics and Genome Sciences, UConn Health, Farmington, CT 06030, USA

[5]Department of Molecular Biology and Biophysics, University of Connecticut School of Medicine (UConn Health), Farmington, CT 06030, USA

[6]Laboratory of Molecular Biology, Department of Synthetic Chemistry and Biological Chemistry, Graduate School of Engineering, Kyoto University, Kyoto 615-8510, Japan

[7]Departments of Biochemistry and Molecular Biology, The Pennsylvania State University College of Medicine, P.O. Box 850, Hershey, PA 17033, USA

[8]Lead contact

SUMMARY

N-methyl-D-aspartate receptor (NMDAR)-mediated glutamate excitotoxicity significantly contributes to ischemic neuronal death and post-recanalization infarction expansion. Despite tremendous efforts, targeting NMDARs has proven unsuccessful in clinical trials for mitigating brain injury. Here, we show the discovery of an interaction motif for transient receptor potential melastatin 2 (TRPM2) and protein kinase Cγ (PKCγ) association and demonstrate that TRPM2-PKCγ uncoupling is an effective therapeutic strategy for attenuating NMDAR-mediated excitotoxicity in ischemic stroke. We demonstrate that the TRPM2-PKCγ interaction allows TRPM2-mediated Ca^{2+} influx to promote PKCγ activation, which subsequently enhances

*Correspondence: lyue@uchc.edu.

AUTHOR CONTRIBUTIONS

L.Y. perceived the project. P.Z. designed and performed most of the *in vitro* experiments and drafted the manuscript. J.F. and Z.Y. performed the majority of the *in vivo* experiments. N.L. and C.X.L. helped to prepare some reagents and edited the manuscript. Y.L. and B.H. helped perform the *in vitro* binding assay and edited the manuscript. B.M. and Y.M. generated TRPM2-KO mice. P.Z. and L.Y. wrote the manuscript, and all authors commented and edited the manuscript.

DECLARATION OF INTERESTS

P.Z. and L.Y. have a pending UConn provisional patent entitled "TRANSIENT RECEPTOR POTENTIAL MELASTATIN 2 (TRPM2) MODULATORS AND USES THEREOF," filed on December 29, 2023, as US application no. 63/615,815.

SUPPLEMENTAL INFORMATION

Supplemental information can be found online at https://doi.org/10.1016/j.celrep.2024.113722.

TRPM2-induced potentiation of extrasynaptic NMDAR (esNMDAR) activity. By identifying the PKCγ binding motif on TRPM2 (M2PBM), which directly associates with the C2 domain of PKCγ, an interfering peptide (TAT-M2PBM) is developed to disrupt TRPM2-PKCγ interaction without compromising PKCγ function. M2PBM deletion or TRPM2-PKCγ dissociation abolishes both TRPM2-PKCγ and TRPM2-esNMDAR couplings, resulting in reduced excitotoxic neuronal death and attenuated ischemic brain injury.

Graphical abstract

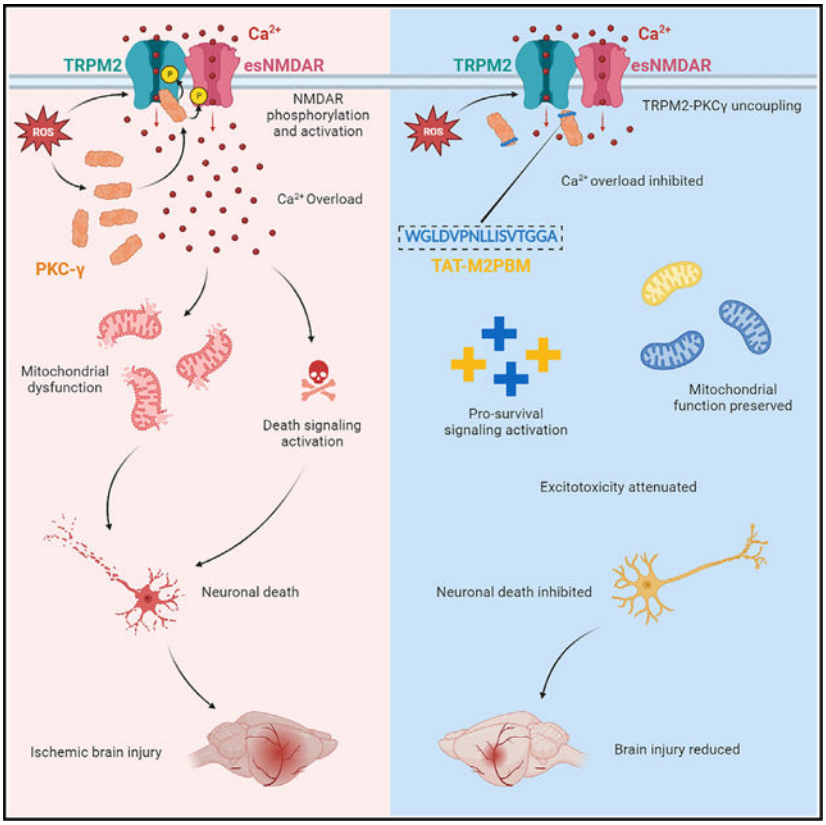

In brief

Zong et al. reveal that the C2 domain of PKCγ directly interacts with the PBM of TRPM2. The TRPM2-PKCγ interaction not only promotes PKCγ activation but also enhances NMDAR-induced ischemic excitotoxicity during stroke. Uncoupling TRPM2-PKCγ association using a small interfering peptide, TAT-M2PBM, mitigates ischemic brain injury in mice.

INTRODUCTION

Ischemic stroke is a leading cause of death and disability globally, with an increasing prevalence in developing countries.[1] N-methyl-D-aspartate receptor (NMDAR)-mediated glutamate excitotoxicity has been known to be the major cause of ischemic neuronal death for decades.[2] However, NMDAR antagonists all unfortunately failed to show protective effects in human patients, which was due to the limited understanding of the pathological

regulation of NMDAR during ischemic stroke.[3,4] Based on their location, NMDARs are divided into synaptic NMDARs (sNMDARs) and extrasynaptic NMDARs (esNMDARs).[5] During ischemic stroke, sNMDARs promote neuron survival, while esNMDARs cause neuronal death.[5] Thus, the indiscriminable blockade of both sNMDARs and esNMDARs is one of the major reasons for the failure of NMDAR antagonists. However, due to the significant similarities between sNMDARs and esNMDARs, developing an esNMDAR-specific antagonist is a significant challenge, if it is possible.

Previously, we reported that the physical and functional coupling between TRPM2 and esNMDAR is important in magnifying ischemic excitotoxicity.[6] TRPM2 is an oxidative-stress-activated, Ca^{2+}-permeable, and non-selective cation channel highly expressed in the brain.[7,8] TRPM2 knockout (KO) was shown to attenuate neuronal death, whereas the underlying molecular mechanisms were elusive.[7] Protein kinase C (PKC) is an important promotor of ischemic brain injury, and PKC inhibition reduces ischemic excitotoxicity.[9,10] PKCγ, the neuron-specific PKC isoform, potentiates NMDAR activity by increasing the surface trafficking of NMDAR and enhancing the channel activity of NMDAR.[11] PKCγ is rapidly activated after ischemic stroke, and KO of PKCγ results in reduced infarction size.[9] However, the mechanisms of the membrane docking and activation of PKCγ in ischemic stroke and the role of PKCγ in esNMDAR-mediated excitotoxicity remain poorly studied.[12]

We recently observed that PKCγ physically associates with the N tail of TRPM2.[6] The recruitment of PKCγ to TRPM2 can be promoted by oxidative stress and during ischemic stroke, but the pathological significance of this binding was still unclear.[6] In this study, we discovered that the C2 domain of PKCγ directly associates with TRPM2 through an interacting motif on TRPM2, the PKC binding motif (M2PBM), which is responsible for physical and functional coupling between TRPM2 and PKC as well as for esNMDAR-mediated excitotoxicity during ischemic stroke. We found that TRPM2-induced potentiation of esNMDAR depends on TRPM2-PKCγ coupling. Moreover, we demonstrated that TRPM2-mediated Ca^{2+} influx promotes PKCγ activation, and vice versa, PKCγ phosphorylates TRPM2 and enhances TRPM2 activation. Furthermore, deleting the binding motif M2PBM in TRPM2 disrupts the physical and functional coupling of TRPM2-PKCγ. Most importantly, we developed an interfering peptide (TRPM2-derived PBM [TAT-M2PBM]) and found that TAT-M2PBM abolishes the functional TRPM2-PKCγ and the TRPM2-esNMDAR couplings, suggesting that TRPM2 serves as an anchor for priming activated PKCγ at the cell membrane during ischemic stroke. Intriguingly, TRPM2-PKCγ uncoupling by TAT-M2PBM attenuates excitotoxicity and neuronal death *in vitro* and *in vivo*. Our results indicate that the TRPM2-PKCγ-esNMDAR complex plays a critical role in ischemic neuronal death and that TRPM2-PKCγ uncoupling is an effective therapeutic strategy specifically targeting esNMDARs for ischemic stroke.

RESULTS

PKCγ phosphorylates TRPM2 and enhances TRPM2 activation

PKC is an important regulator of ion channel activity.[13] Previously, we reported that PKCγ binds to TRPM2, but whether this binding influences TRPM2 activity was not clear.[6] As PKCγ is regarded as a neuron-specific PKC isoform, we examined the endogenous PKCγ

expression in HEK293T cells using western blot analysis. The results showed that although very low, there was still detectable PKCγ expression in HEK293T cells (Figures S1A and S1B). Thus, we overexpressed PKCγ in all the experiments performed in HEK293T cells. We found that the PKCγ activator phorbol 12-myristate 13-acetate (PMA) induced TRPM2 activation in HEK293T cells overexpressing with TRPM2 and PKCγ using the internal pipette solution containing 1 μM ADP ribose (ADPR) and 500 nM Ca^{2+} (Figure 1A). Moreover, a 3-min H_2O_2 preincubation enhanced the PMA-induced TRPM2 activation (Figures 1B and 1C), consistent with our previous findings that oxidative stress promotes the binding of PKCγ to TRPM2.[6] However, PMA failed to induce TRPM2 activation in the TRPM2/EGFP control (Figure 1D) and the TRPM2/PKCγ-DN (dominant-negative kinase-dead PKCγ) (Figure 1E) groups even after H_2O_2 preincubation, suggesting that PMA regulates TRPM2 activation in a PKCγ-dependent manner.

PKC regulates ion channel functions through direct phosphorylation or influencing the membrane phosphatidylinositol (4,5) bisphosphate level.[13] We performed mass spectrometry analysis to detect the potential phosphorylation of TRPM2 by PKCγ and found that PMA induced the phosphorylation of TRPM2 at serine 11 and 38 (S11 and S38) (Figures S1C and S1D), both of which match conserved PKC consensus phosphorylation motif (RKxxS, RRxxS).[14] Protein sequence alignments show that S11 and S38 only present in TRPM2 among all the human TRPM channels (Figure S2A), and S38 of TRPM2 is highly conserved in TRPM2 of different species (Figure S2B). To determine whether S11 or S38 phosphorylation is responsible for the activation of TRPM2 by PMA, we mutated S to alanine (A) at S11 and S38 to abolish their phosphorylation (Figure 1F) and found that the S11A mutation did not influence the activation of TRPM2 by PMA, whereas the S38A mutation eliminated this activation (Figures 1G, 1H, and 1K). To further confirm the potentiation of S11/38 phosphorylation in TRPM2 activation, we mutated S to aspartate (D) at S11 and S38 to create the “phosphomimetic” mutants (Figure 1F). We found that the S38D mutation led to the activation of TRPM2 without perfusion of PMA under the same recording condition, which was not seen in the S11D mutation (Figure 1I–1K). This result strongly suggests that phosphorylation of TRPM2 at S38, but not at S11, facilitates the activation of TRPM2 when ADPR and Ca^{2+} concentrations are kept at minimal levels that are insufficient for inducing TRPM2 activity without additional stimuli.

The activation of TRPM2 requires both Ca^{2+} and ADPR.[7] Thus, we titrated the concentrations of Ca^{2+} and ADPR in the internal recording solution to 500 nM and 1 μM, respectively, aiming to achieve the minimal activation of TRPM2 at baseline, but a rapid activation of TRPM2 upon PMA treatment (Figure 1L, left). To examine the maximal activation of TRPM2, we increased the concentrations of Ca^{2+} and ADPR in the internal recording solution to 1 mM and 500 μM, respectively (Figure 1L, middle). The results of averaged current amplitude showed that the PMA treatment enhanced the maximal activation of wild-type TRPM2 (TRPM2-WT) but not the S38A mutant (Figure 1M). Moreover, PMA did not further increase the activation of the S38D mutant (Figure 1M), and mutation of S11 to either A or D did not influence the activation of TRPM2 (Figure 1N). Thus, it appears that S38 phosphorylation by PMA mediates PKCγ-induced TRPM2 activation. As S38 is conserved in TRPM2 from different species (Figure S2B), the drastic

regulation of TRPM2 activation by PMA through the S38 phosphorylation site suggests that the S38 of TRPM2 may play an important role in the evolution.

Then, we sought to determine whether S11/38 phosphorylation influences the potentiation of NMDAR currents by TRPM2. To eliminate any potential contamination from the activation of TRPM2 during NMDAR current recording, we added a potent Ca^{2+} chelator, BAPTA, into the internal pipette recording solution, which does not contain any ADPR (Figure 1L, right). Consistent with our previous findings,[6] co-expression with TRPM2 increased the amplitude of NMDAR currents (Figures 1O and 1P). However, mutation of S11/38 to A and D did not affect the potentiation of TRPM2 on the channel activity of NMDAR (Figures 1O and 1P), suggesting that phosphorylation of TRPM2 by PMA is not required for the functional coupling between TRPM2 and NMDAR under this recording condition, although we cannot exclude the possibility that it may enhance TRPM2-NMDAR coupling under oxidative stress conditions.

TRPM2-mediated Ca^{2+} influx promotes PKCγ activation

The activation of PKCγ requires Ca^{2+},[15] and TRPM2 is permeable to Ca^{2+}.[16] Considering the strong physical binding between TRPM2 and PKCγ induced under oxidative stress conditions,[6] we hypothesized that TRPM2 may be an important Ca^{2+} source for PKCγ activation. The C kinase activation reporter (CKAR) is a sensitive sensor that can be used for real-time detection of PKC activity.[17] PKC activation induces conformational changes of the CKAR, which abolishes the basal fluorescence resonance energy transfer (FRET) inside CKAR, as reflected by the reduced FRET intensity and increased CFP/YFP ratio (Figure 2A). We found that H_2O_2 perfusion at 100 mM induced a stronger activation of PKCγ in HEK293T cells co-expressed with both TRPM2 and PKCγ compared to PKCγ single-expressed cells (Figures 2B–2D), suggesting that TRPM2 promotes PKCγ activation under oxidative stress conditions. We further assessed the role of TRPM2-mediated Ca^{2+} influx in PKCγ activation (Figure 2E) and found that the TRPM2 blocker N-(*p*-amylcinnamoyl) anthranilic acid (ACA)[18] eliminated the increase of PKCγ activation induced by TRPM2 (Figures 2F–2H). Moreover, buffering of extracellular Ca^{2+} influx using EGTA or chelating of intracellular Ca^{2+} using BAPTA (AM) completely abolished the activation of PKCγ by H_2O_2 in TRPM2/PKCγ co-expressed cells (Figures 2F–2H). These results suggest that TRPM2-mediated Ca^{2+} influx promotes PKCγ activation under oxidative stress conditions.

Physical and functional coupling between TRPM2 and PKCγ

As Ca^{2+} entering from the extracellular environment is quickly chelated by endogenous intracellular Ca^{2+} buffering proteins, including parvalbumins, calbindin, and calretinin,[19] to effectively supply PKCγ with Ca^{2+}, TRPM2 must need to be located in close proximity to PKCγ. Although we have previously found that TRPM2 binds to PKCγ using co-immunoprecipitation,[6] whether the binding between TRPM2 and PKCγ is a direct association or mediated by an adaptor protein remains unclear. Thus, we decided to locate the binding site at TRPM2 for PKCγ. We found that the amino acid sequence (WGLDVPNLLISVTGGA) at an area near the N terminus of TRPM2 highly resembles several known PKCγ binding sequences, including the ones in RACK1 (DIINALC) and annexin1 (KGDYEKILVALCGGN) (Figure 3A),[20] which both bind to the C2 domain of

PKC.[21] All other TRPM channels, except TRPM8, share a similar consensus sequence (~50%) in this area (Figure S3A), which is also highly conserved in the TRPM2 from different species (Figure S3B). Importantly, after deletion of this sequence area, the physical interaction between TRPM2 and PKCγ was abolished (Figure 3B), and this deletion did not affect the expression of TRPM2 in HEK293T cells (Figures S3C and S3D). This result underscores a critical role of this sequence motif in the physical coupling of PKCγ and TRPM2. We therefore designated this sequence area "TRPM2-PKC binding motif" (M2PBM) (Figure 3C).

To further determine whether the association between TRPM2 and PKCγ is a direct binding or requires an additional adapter protein, we purified the MHR1/2 domain of TRPM2 and the C2 domain of PKCγ and performed *in vitro* binding experiments as we previously reported (Figures S3E and S3F).[6] After incubation in binding buffer for 24 h, compared to the negative control of GST protein, we could use the C2 domain of PKCγ (tagged with GST) to immunoprecipitate the MHR1/2 domain of TRPM2 (tagged with His_6) (Figure 3D), suggesting that the PBM of TRPM2 can directly interact with the C2 domain of PKCγ.

We then attempted to determine whether M2PBM is required for the functional coupling between TRPM2 and PKCγ. Whole-cell current recording showed that PMA failed to induce the activation of TRPM2 with PBM deletion (TRPM2-ΔPBM) (Figures 3E and 3F), as the average basal current amplitude of the PMA-perfusion group was similar to that of non-PMA-treated groups (0.26 ± 0.05 nA, $n = 7$, $p > 0.05$). Similarly, deletion of the PBM eliminated the increase of PKCγ activation by TRPM2 upon H_2O_2 treatment (Figures 3G–3I). These results suggest that the functional coupling between TRPM2 and PKCγ depends on their physical association. More importantly, the potentiation of NMDARs by TRPM2-WT could not be replicated by TRPM2-ΔPBM (Figures 3J and 3K), suggesting that the functional coupling between TRPM2 and NMDAR requires the direct binding of PKCγ to TRPM2.

TAT-M2PBM abolishes TRPM2-PKCγ and TRPM2-NMDAR coupling

To further confirm the role of TRPM2-PKCγ physical binding via M2PBM in the functional coupling of TRPM2-PKCγ as well as the functional coupling of TRPM2-NMDAR, we synthesized a membrane-permeable peptide TAT-M2PBM and used it as a tool to dissociate the binding between TRPM2 and PKCγ (Figure 4A).[5,6,22] We found that TAT-M2PBM incubation at 1 μM for 2 h effectively prevented the pulling down of PKCγ by anti-TRPM2, indicating that TAT-M2PBM inhibited the TRPM2-PKCγ interaction (Figure 4B). Importantly, when used at 1 mM, TAT-M2PBM did not significantly affect PKCγ activity *in vitro* (Figure S3G). Moreover, the PMA-induced activation of TRPM2 currents in PKCγ/TRPM2 co-expressed cells (Figures 4C and 4D), as well as the enhancement of PKCγ activity by TRPM2 during H_2O_2 perfusion (Figures 4E and 4F), was abolished by TAT-M2PBM, indicating that TAT-M2PBM is effective in disrupting the functional coupling of TRPM2-PKCγ. Furthermore, TAT-M2PBM suppressed TRPM2-induced potentiation of NMDAR currents (Figures 4G and 4H). These results validated a critical role of M2PBM in TRPM2-PKCγ coupling and the indispensable role of physical TRPM2-PKCγ binding in functional coupling of TRPM2-PKCγ as well as TRPM2-NMDARs.

We next examined the effect of TAT-M2PBM on TRPM2-NMDAR coupling in cortical neurons isolated from WT and *Trpm2* deletion (M2KO) mice. Compared to WT neurons, we recorded smaller NMDAR currents in M2KO neurons (Figures 4I and 4J) as we previously reported.[6] Importantly, TAT-M2PBM preincubation effectively inhibited NMDAR current amplitude in WT neurons to a level similar to that in M2KO neurons (Figures 4I and 4J). Consistent with current recording results obtained in neurons, the increase of NMDAR's surface expression induced by co-expression with TRPM2 and PKCγ in HEK293 cells was inhibited by TAT-M2PBM preincubation (Figures 4K and 4L).

Since TRPM2-mediated Ca^{2+} influx is a strong promotor of PKCγ activation (Figure 2), and since PKCγ is an important activator of NMDAR,[4,11] we evaluated whether TAT-M2PBM affects the regulation of NMDAR activity by PKCγ. A 60-s perfusion of PMA markedly increased NMDAR current amplitude in WT neurons but not in M2KO neurons (Figure 4M, left, 4N, and 4O). Similarly, we found that TAT-M2PBM effectively inhibited the enhanced NMDAR activity by PMA in WT neurons and produced a similar effect to TRPM2 KO (Figure 4M, right, 4N, and 4O), suggesting that TRPM2-PKCγ interaction enhances NMDAR activity.

TRPM2-PKCγ uncoupling protects neurons against OGD

As uncoupling of TRPM2-PKCγ by TAT-M2PBM inhibited the potentiation of NMDARs by TRPM2, we reasoned that TAT-M2PBM may protect against NMDAR-mediated excitotoxicity. Thus, we examined whether TAT-M2PBM attenuates oxygen glucose deprivation (OGD)-induced ischemic neuronal injury.[6,23]

As Ca^{2+} overload is a critical cause of ischemic neuronal death,[24] we used real-time ratio Ca^{2+} imaging for detecting Ca^{2+} overload during OGD perfusion.[6,22] We found that TAT-M2PBM preincubation for 2 h at 1 μM effectively inhibited the increase of intracellular Ca^{2+} concentration (Figures 5A–5C) as well as neuronal death (Figure 5D) during OGD, a potent protective effect that was similar to that produced by the NMDAR antagonists MK801/AP5 and M2KO (Figures 5A–5D), indicating that Ca^{2+} overload as well as NMDAR-mediated excitotoxicity was inhibited by TAT-M2PBM. As TRPM2 is an oxidative-stress-activated ion channel, and as the phosphorylation by PKCγ may enhance the activity of TRPM2 under ischemic conditions, we also evaluated whether TAT-M2PBM protects H_2O_2-induced neuronal death. We found that when perfused continuously at 100 μM, H_2O_2 induced rapid Ca^{2+} overload and neuronal death in WT cortical neurons treated with TAT-SC, while the incubation of TAT-M2PBM effectively attenuated this cytotoxic effect (Figures S4A–S4D). This result suggests that the PKC phosphorylation may be an important contributor for TRPM2 activation under oxidative stress conditions, and that TAT-M2PBM can protect neuronal death caused by the stress factors beyond NMDAR-mediated excitotoxicity.

Since nitric oxide (NO) production caused by energy imbalance during ischemic stroke is an important promoter for neuronal death,[25] we measured NO production using DAF-FM in neurons subjected to OGD.[26] We found that OGD caused a substantial increase of NO concentration in WT neurons, which was inhibited by TAT-M2PBM, MK801/AP5, and M2KO (Figures 5E and 5F), suggesting that TAT-M2PBM attenuated the NO toxicity caused by OGD in WT neurons. As reactive oxygen species (ROS) is an initiator and mediator

of ischemic neuronal death,[27] we used MitoSOX to evaluate ROS generation in neurons during OGD.[28] We found that the increase of MitoSOX in WT neurons induced by OGD was inhibited by TAT-M2PBM, MK801/AP5, and M2KO (Figures 5G and 5H), suggesting that ROS production was attenuated by uncoupling of TRPM2 and PKCγ. As shutting down the energy supply caused by mitochondrial dysfunction is an early sign of neuronal death during ischemic stroke,[29] we evaluated mitochondria function using Rhodamine 123 (R123), a heavily positively charged dye that becomes self-dequenched upon attracted to mitochondria[30] and gets released from depolarized mitochondria during mitochondrial stress.[5,6,22] We observed that OGD induced a marked increase of R123 florescence in WT neurons but not in WT neurons treated with TAT-M2PBM or MK801/AP5 or in M2KO neurons (Figures 5I and 5J), suggesting that mitochondrial function was preserved by TAT-M2PBM.

In summary, the above data indicate that uncoupling of TRPM2-PKCγ attenuates ischemic neuronal dysfunction and death. It is noteworthy to mention that TAT-M2PBM did not produce any additional protective effect in neurons from M2KO mice, indicating the specificity of TAT-M2PBM in disrupting TRPM2-PKCγ association.

TAT-M2PBM attenuates ischemic stroke

After confirming the protective effect of TRPM2-PKCγ uncoupling against ischemic neuronal death *in vitro*, we sought to evaluate the therapeutic value of TAT-M2PBM using transient middle cerebral occlusion (MCAO) in mice. In order to determine the administration dosage and frequency, we first examined the *in vivo* disruption efficiency of TAT-M2PBM. Intraperitoneal (i.p.) injection was selected as the delivery method due to the efficient absorption of cell-penetrating peptides (CPPs) through this route.[31] As shown in Figure 6A, TAT-M2PBM eliminated the physical association between TRPM2 and PKCγ in the mouse brain as early as 2 h after the i.p. injection at a dose of 100 nmol/kg, and this disruption can be maintained for at least 12 h (Figure 6A). Importantly, TAT-M2PBM did not influence the binding between TRPM2 and NMDARs (Figure 6A). We therefore designed the administration strategy as shown in Figure 6B to mimic the clinical setting: an injection was given 2 h after MCAO and right before the reperfusion, and then after 12 h, another i.p. injection was given to maintain the disruption until the harvest of brains 24 h after reperfusion (Figure 6B). We found that TAT-M2PBM reduced the infarction size and prevented the impairment of the neurological deficient (ND) score 24 h after MCAO reperfusion in WT mice but did not produce any additional protective effect in M2KO mice (Figures 6C and 6D). More-over, the increased surface expression of NMDARs in WT mice after MCAO was inhibited by TAT-M2PBM (Figures S5A and S5B). Furthermore, we compared the *in vivo* protective effect of TAT-M2PBM with our previously reported TAT-EE_3, which functions by dissociating the TRPM2-NMDAR complex.[6] The results showed that compared to TAT-EE_3, TAT-M2PBM treatment reduced brain damage, although there was no difference in ND score between the two groups (Figures 5E and 5F). As NMDAR is predominantly expressed in neuronal cells, our data suggest that compared to NMDAR blockers and TAT-EE_3, TRPM2-PKCγ uncoupling may produce a broader protective effect by attenuating ischemia-induced dysfunction and damage in other cell types. We then examined the long-term protective effects of TAT-M2PBM and found that

TAT-M2PBM effectively reduced brain injury and preserved brain function (also reflected by rotarod test) 7 days after MCAO (Figures 5H–5K). The above results indicate that TRPM2-PKCγ coupling plays a pivotal role in mediating NMDARs' excitotoxicity and neuronal death during ischemic stroke.

In conclusion, during ischemic stroke, ROS promotes the binding of PKCγ to the TRPM2-NMDAR complex,[6] which leads to phosphorylation and activation of TRPM2, and enhanced NMDARs' activity. Meanwhile, our data suggest a scenario in which TRPM2-mediated Ca^{2+} influx enhances the activation of PKCγ, which further increases NMDAR-mediated excitotoxicity, neuronal death, and brain injury (Figure 6G, left). In contrast, TAT-M2PBM selectively inhibits the binding of PKCγ to TRPM2, resulting in an effective suppression of the potentiated NMDAR activity and producing a potent protective effect against neuronal death and ischemic brain injury (Figure 6G, right). Our study suggests that uncoupling of TRPM2-PKCγ interaction represents a promising therapeutic strategy for screening effective treatments for ischemic stroke.

DISCUSSION

Decades after the demonstration of the critical role of glutamate excitotoxicity in ischemic stroke, there is still no therapy available for attenuating ischemic brain injury through targeting the culprit of excitotoxicity, NMDARs. One of the significant challenges for developing neuroprotectants by targeting NMDARs is to selectively inhibiting esNMDARs, which is almost mission impossible using pharmacological approaches. Here, we show that functional coupling of TRPM2-PKCγ is necessary for NMDAR-mediated excitotoxicity in ischemic stroke. More importantly, we demonstrate that TAT-M2PBM, a cell-permeable peptide that disrupts TRPM2-PKCγ coupling, markedly inhibits esNMDAR-mediated excitotoxicity and exhibits potent protective effect against ischemic brain injury. Our study provides proof of concept that approaches that keep the associating proteins away from esNMDARs represent a promising direction for developing therapeutics for ischemic stroke.

TRPM2 and PKCγ functional coupling is necessary for TRPM2-NMDAR-coupling-mediated excitotoxicity

Using mass spectrometry analysis, we identified the PKCγ phosphorylation sites in TRPM2 and found that PKCγ-mediated phosphorylation regulates TRPM2 channel activity. Phosphorylation of TRPM2 has been shown in previous studies.[32,33] The first evidence of phosphorylation-mediated regulation of TRPM2 was that tyrosine phosphatase PTPL1 inhibited the phosphorylation of TRPM2 and reduced the increase of intracellular Ca^{2+} concentration following a 5-min H_2O_2 treatment.[32] In another study, H_2O_2 treatment was shown to increase the phosphorylation of the TRPM2 short variant (TRPM2-S), but not the full-length TRPM2, at S39 in endothelial cells, which can be abolished by a specific PKCα inhibitor.[33] It remains unknown why the full-length TRPM2 was not phosphorylated[33] since TRPM2-S and TRPM2 share an identical amino acid sequence near the phosphorylation site.[33] As both previous studies used Ca^{2+} imaging to assess TRPM2 channel activity changes by PKC phosphorylation,[32,33] we applied current recordings of TRPM2 to directly evaluate how phosphorylation of TRPM2 regulates channel activity. We found that PKCγ-

induced phosphorylation, as well as phosphomimetics mutation of TRPM2, drastically potentiated TRPM2 channel activity, suggesting a functional significance of phosphorylation of TRPM2 by PKCγ under physiological or pathological conditions.

Using mutagenesis approaches, a recent study demonstrated that treatment of PKC activator PMA at 100 nM for 1 to 6 h increased the phosphorylation of TRPM2 at T738, which led to inhibited TRPM2 activation and elevated the temperature threshold for TRPM2 activation.[34] We did not identify the T738 phosphorylation site using mass spectrometry. In our experiments, we used a 5-min PMA treatment to induce phosphorylation, as phosphorylation happens within minutes, whereas Kasshio and colleagues induced phosphorylation for 1 to 6 h with 100 nM PMA. The different duration of PMA treatment could have contributed to the discrepancy of phosphorylation status at T738 in our and their studies.[34] Nonetheless, the potentiation of TRPM2 activity by PKC phosphorylation detected by current recordings in our study is supported by the previous report, which showed enhanced TRPM2-mediated Ca^{2+} influx by phosphorylation.[32]

The activation of PKCγ during ischemic stroke and the potentiation of NMDARs directly by PKCγ have been well documented. During early ischemic injury, PKCγ can be quickly activated and regulates NMDAR activity by directly phosphorylating NMDARs, thereby increasing neuronal death.[9] Our previous data suggest that PKCγ recruited to the TRPM2-NMDAR complex may be necessary for TRPM2-mediated increase of NMDAR activity during ischemic stroke. Here, we found that the physical interaction of PKCγ with TRPM2 is not only required for PKCγ-induced potentiation of TRPM2 activity but also leads to enhanced activity of PKCγ, as the close vicinity of PKCγ to TRPM2 brings itself a reliable Ca^{2+} source for its own activation. Our results suggest that during ischemic stroke, uncoupling of TRPM2-PKCγ association will inhibit functional coupling of esNMDAR-TRPM2 and diminish the esNMDAR-mediated excitotoxicity.

Uncoupling of TRPM2 and PKCγ is sufficient to attenuate excitotoxicity in ischemic stroke

We identified a PKCγ binding motif (M2PBM) in the MHR1 domain of the N tail of TRPM2, which particularly resembles the sequence motifs in RACK1 and annexin1 for binding to the C2 domain of PKC.[21] This could explain why we observed an increased binding of PKCγ to TRPM2 after H_2O_2 treatment and ischemic stroke[6]: activation of PKCγ during oxidative stress exposes the C2 domain[12] and allows its binding to TRPM2, which may “lock” the PKCγ in the activated state. Conventional PKCs (α, β, and γ) share highly conserved sequences,[12] suggesting that PKCα and PKCβ may also interact with TRPM2 through the same binding motif, M2PBM. However, this will not cause non-specific or off-target effects in the peripheral tissues since TRPM2-NMDAR-mediated excitotoxicity only happens in neuronal cells where NMDARs are localized. It will be of great interest to investigate whether other conventional PKCs including PKCα and PKCβ interact with TRPM2 in future studies.

The most important discovery of this study is the effects of disrupting peptide TAT-M2PBM, which effectively interferes with PKCγ-TRPM2 coupling as well as with TRPM2-NMDAR functional coupling, attenuates excitotoxicity, and produces potent protective effects against ischemic stroke *in vitro* and *in vivo*.

An effective strategy in targeting NMDAR for treatment of ischemic stroke

NMDAR-mediated glutamate excitotoxicity is the culprit of ischemic neuronal death.[2] One of the major reasons for the past failures of NMDAR antagonists in the treatment of clinical ischemic stroke is their non-selective blockade on both the "beneficial" sNMDAR and the "detrimental" esNMDAR.[3] Selectively inhibiting the neurotoxic effects of esNMDARs without impairing the critical physiological and pro-survival functions of sNMDARs represents an effective strategy of developing more effective NMDAR antagonists for neuroprotectants to treat ischemic stroke.[3] However, sNMDARs and esNMDARs share similar components and structures, and current pharmacological technology is not able to develop an NMDAR antagonist that is selective for esNMDARs. Thus, targeting the "accomplices" of esNMDAR, which specifically enhance esNMDAR activity during ischemic stroke, is an innovative way to achieve the selective inhibition on the excitotoxic esNMDAR.

Our previous findings show that TRPM2 is only expressed at the extrasynaptic sites and specifically enhances the activity of esNMDARs but not sNMDARs.[6] In this study, our results present a functional TRPM2-PKCγ-esNMDAR complex at extrasynaptic sites in ischemic injury. During ischemic stroke, oxidative stress activates TRPM2 and promotes the binding of PKCγ to TRPM2, leading to enhanced TRPM2 channel activity and TRPM2-mediated Ca^{2+} influx, which in turn becomes a reliable Ca^{2+} source for PKCγ activation. PKCγ phosphorylation and activation of TRPM2 and subsequent activation of PKCγ by TRPM2-mediated Ca^{2+} form a positive feedback loop to perpetuate PKCγ activation. Consequentially, by directly associating with NMDARs, TRPM2 serves as a scaffold to recruit the activated PKCγ to its substrate, NMDARs, in the TRPM2-PKCγ-esNMDAR complex, leading to substantial potentiation of esNMDAR-mediated excitotoxicity. Interfering peptide TAT-M2PBM effectively disrupts TRPM2-PKCγ coupling, thereby protecting mice against ischemic stroke.

In summary, our results provide proof of concept that targeting the TRPM2-PKCγ-esNMDAR complex by keeping the "accomplices" apart is a promising direction to develop better therapeutics for ischemic stroke. Our study will also shed light on future strategies of mitigating neuronal injury by selectively inhibiting the detrimental activity of esNMDARs in various neurodegenerative diseases.

Limitations of the study

While our study demonstrated the intriguing protective effect of uncoupling the TRPM2-PKCγ interaction using TAT-M2PBM against ischemic stroke, several issues warrant further investigation. First, although we have shown that TRPM2-PKCγ interaction promotes increased activity of TRPM2 and PKCγ in the *in vitro* experiments, the subsequent pathological consequences *in vivo* in the ischemic stroke requires further investigation. Second, to further understand the physiological/pathological significance of TRPM2 and PKCγ functional coupling, future experiments need to evaluate TRPM2 activity using current recordings in brain slices from MCAO mice, which will provide additional insights into how the inhibition of TAT-M2PBM on TRPM2 activation plays a role in ischemic stroke. Third, while the current study focused on the TRPM2-PKCγ interaction, given the

homology sequences of the C2 domain in different classical PKC isoforms, it is worthy of investigating whether TRPM2 interacts with other classical PKC isoforms and the potential physiological/pathological consequences. Fourth, the better protective effects of TAT-M2PBM than those of TAT-EE_3 (Figures 6E and 6F) suggest that TAT-M2PBM may mediate protective effects in addition to NMDAR-caused excitotoxicity, which is likely in non-neuronal cells. Therefore, it is of great interest to investigate the role of the coupling of TRPM2 with other PKCs, including PKCα and PKCβ, in non-neuronal cell types in ischemic stroke. This may lead to the development of a therapeutic peptide with better and broader protective effects against ischemic stroke. Fifth, we used male mice in the current study since a previous report suggested that inhibition of TRPM2 only protected neuronal death in male mice.[35] Since we have shown that TAT-M2PBM can effectively protect mice against ischemic stroke and that non-neuronal cells also likely contribute to the protective effects, one of our future projects is to thoroughly investigate the effects of TAT-M2PBM against ischemic stroke in female mice in comparison to male mice so that we can provide translational insights that TAT-M2PBM is a potential therapy with a broader range of effectiveness for both males and females. Lastly, as one of the CPP-conjugated peptides, although TAT-M2PBM has been shown to be effective in protecting against both acute and chronic ischemic stroke (Figure 6), further investigation regarding its stability, safety, and pharmacokinetics is warranted for its translational application. CPP-conjugated peptides can be effectively administrated by i.p. injection, intravenous injection, transdermal administration, intranasal administration, and transcutaneous administration.[36] For i.p. injection, it has been demonstrated in great detail by using the GFP-fused TAT-BNDF regarding the speed of absorption, distribution, and pharmacokinetics.[37] Moreover, similar to our chronic studies, animals (mice and rats) were i.p. injected with GFP-fused TAT-BNDF daily[37] for 1 month before behavioral testing, and no abnormality caused by TAT peptide was shown.[37] TAT peptide and other CPP cargoes enter cells by one of two mechanisms: micropinocytosis (endocytosis) or by direct membrane transduction (direct translocation) via direct penetration at specific sites where small particle-like cell surface structures are formed.[38] Although it has been shown *in vitro* that the commonly used CPPs are passive carriers that do not initiate an innate immune response in epithelial cells or induce any epithelial-cell-associated “danger signals” during the process of cytoplasmic delivery of a model protein cargo,[39] caution needs to be taken for potential *in vivo* immune responses and toxicity. CPP-conjugated drugs have been widely used in diagnosis and treatment in both preclinical experiments and clinical trials.[36] However, up to date, none of them have been approved by the FDA, possibly due to issues such as immunogenicity, cellular toxicity, low specificity, and endosomal degradation.[36] Thus, designing and optimizing TAT-M2PBM to be safe, efficient, and more specific holds great promise for its successful application in ischemic stroke.

STAR★METHODS

RESOURCE AVAILABILITY

Lead contact—Further information and requests for resources and reagents should be directed to and will be fulfilled by the lead contact Lixia Yue (lyue@uchc.edu).

Materials availability—This study did not generate new unique reagents.

Data and code availability

- All original data will be available upon contacting Lixia Yue (lyue@uchc.edu).
- This paper does not report original code.
- Any additional information required to reanalyze the data reported in this work paper is available from the lead contact upon request.

EXPERIMENTAL MODEL AND STUDY PARTICIPANT DETAILS

Animals—All the experimental mice bred and hosted in the animal facility building of University of Connecticut School of Medicine (UCONN Health) were fed with standard chow diet and water *ad libitum*. Standard housing conditions were maintained at a controlled temperature with a 12-h light/dark cycle. All experimental procedures and protocols were approved by the Institutional Animal Care and Use Committee (IACUC) of University of Connecticut School of Medicine (animal protocol: AP-200135–0723), and were conduct-ed in accordance with the U.S. National Institutes of Health Guidelines for the Care and Use of Laboratory Animals. 8 to 12 weeks old male mice were used in this study. The reason why we only used male mice was explained in the discussion section.

The global TRPM2 knockout (TRPM2-KO, or gM2KO) mice were generated by Dr. Yasuo Mori's lab at Kyoto University Japan. The deletion of *Trpm2* was developed in C57B6J mouse by replacing the third exon (S5–S6 linker in the pore domain) with a neomycin coding region. The knockout mice exhibited no differences in behavior or impairment in breeding, compared to wild type (WT) C57BJ6 mice.[44] TRPM2-KO mice were back-crossed to C57BL/6 mice for ≥10 generations before being used for experiments.

Cortical neuron isolation and culture—Mice pups at P0 were euthanized based on animal protocol. Whole brain was harvested and immersed in frozen Hank's Balanced Salt Solution (HBSS). Meninges were peeled. Brain stem and thalamus were removed. Cortical tissues were cut into small pieces and digested with 0.25% trypsin (Thermal Fisher Scientific, 15090–046) in HBSS at 37°C for 15 min. Tissue pellets are washed with HBSS. Cells were resuspended with appropriate amount of Neurobasal Medium (Thermal Fisher Scientific, 21103–049) supplemented with 2% B27 supplement (Thermal Fisher Scientific, 17504–044), 3% horse serum (Thermal Fisher Scientific, 16050114), 0.25% L-glutamine (Thermal Fisher Scientific, 25030–081) and 1% penicillin/streptomycin (Thermal Fisher Scientific, 15140–122). Isolated cells were counted and plated on coverslips pre-coated with poly-L-lysine (Sigma-Aldrich, P4707) at a density of about 500×10^3 cells/cm^2 for OGD and H_2O_2 treatment, and 100×10^3 cells/cm^2 for current recording. Cytosine arabinoside (Sigma-Aldrich, C1768) was added to maintain a concentration at 1μM to inhibit the proliferation of non-neuronal cells. 24 h after plating, culture medium was changed to Neurobasal Medium supplemented with 2% B27 supplement, 0.25% L-glutamine and 1% penicillin/streptomycin. The concentration of Cytosine arabinoside (araC) was increased to 2 μM. Medium was changed every 3 days. OGD and current recording were performed at 7th day of culture.

Cell line culture and transfection—HEK293T cells were cultured in Dulbecco's Modified Eagle's medium (DMEM) (Thermal Fisher Scientific, 12100–038) supplemented with 10% BGS (HyClone, SH30541.03) and 0.5% penicillin/streptomycin (Thermal Fisher Scientific, 15140–122) at 37°C and 5% CO_2. 2 h prior to transfection, culture medium was replaced with DMEM supplemented with 5% BGS. Cells were transfected when the confluence was about 60% using Lipofectamine 3000 Transfection Kit (Thermal Fisher Scientific, 2232162) based on the manual.

METHOD DETAILS

Middle cerebral artery occlusion (MCAO)—Eight-to nine-week-old male mice (~25 g) were subjected to transient middle cerebral artery occlusion (tMCAO) for 120 min followed by 24 h of reperfusion. The genotype information was blinded to the surgeon who conduct the surgeries. MCAO surgery was performed as previously described.[45,46] In brief, mice were anesthetized based on animal protocol. The unilateral right middle cerebral artery (MCA) occlusion was achieved by inserting a silicone-coated 6–0 monofilament (Doccol Corporation, Sharon, MA) 10 to 11 mm from internal carotid artery bifurcation via an external carotid artery incision.[47] Mouse body temperature was maintained at ~ 37°C (TCA T-2DF, Physitemp). Cerebral blood flow was monitored before and after occlusion as well as after reperfusion. The bregma was exposed and the skull bone countersunk at two 3 × 3-mm areas over both MCA supply territories for bilateral monitoring of local cortical blood flow. Successful occlusion was confirmed by 85% reduction of cerebral blood flow monitored using laser Doppler blood FlowMeter (Moor-VMS-LDF1, Moor Instrument, Dever, UK). Sham control mice underwent the same procedure but without insertion of filament to occlude the MCA.

Neurological deficit score evaluation—Neurological deficit was scored based on previously reported criteria.[48] In brief, score 0 represents no neurological deficit; score 1 represents failure to extend left paw; Score 2 represents circling to the left; score 3 represents falling to the left; score 4 represents inability of spontaneously walking and decreased level of consciousness; and score 5 represents death due to brain ischemia. The observer to score the neurological deficit was an experienced observer and blinded by the group assignment and genotype information. If the animal score was 0 or 5, it was removed from the study.

Rotarod test—For examining the long-term protective effect of TAT-EE3, motor coordination of mice was evaluated by rotarod test right after the evaluation of neurological deficit score at 3rd and 7th day after MCAO. Briefly, mice were placed on a rotating rod with the speed range of 6–56 rounds per minute for 5 min. Each mouse was tested for 3 times with two 20-min interval in between. The falling from the rotating rod was recorded and the averaged latency of each mouse was used for quantification.

Infarct volume assessment by Triphenyl tetrazolium chloride (TTC) staining—Tetrazolium chloride (Sigma-Aldrich, T-8877) was dissolved in PBS at a concentration of 2% 30 min prior to use. Post-stroke mice were euthanized, and brains were frozen at —80°C for 5 min. Brains were cut into coronary slices at a thickness of 1 mm. Brain slices were

stained with 2% TTC (v/v) for 20 min, and then washed using PBS for 3 times, and fixed in 10% Neutral buffered formalin for later scanning. TTC labels non-injured tissue, leaving the infarct area white. The stained slices were scanned for data analysis using ImageJ software. The infarct volume was calculated and presented as a percentage of total brain volume as previously reported.[49,50]

Antibodies, chemicals and reagents—Rabbit polyclonal antibodies to TRPM2 (Novus, NB110–81601, 1:50 in protein extraction for IP); Rabbit polyclonal antibodies to GluN2A (Cell Signaling Technology, 4205S, 1:1000 in 5% BSA for WB). Rabbit polyclonal antibodies to GluN2B (Cell Signaling Technology, 4207S, 1:1000 in 5% BSA for WB); Rabbit polyclonal antibodies to PKC-γ (Cell Signaling Technology, 59090S, 1:5000 in 5% BSA for WB); Rabbit polyclonal antibodies to Pan-cadherin (Cell Signaling Technology, 4068S, 1:5000 in 5% BSA for WB); Rabbit monoclonal antibodies to GAPDH (Cell Signaling Technology, 5174S, 1:5000 in 5% BSA for WB); Rabbit monoclonal antibodies to GST-Tag (Cell Signaling Technology, 2622S, 1:100 for IP); Rabbit monoclonal antibodies to His-Tag (Cell Signaling Technology, 12698S, 1:5000 in 5% BSA for WB); Anti-mouse IgG, HRP-linked Antibody (Cell Signaling Technology, 7076, 1:10000 in 5% BSA for WB); Anti-rabbit IgG, HRP-linked Antibody (Cell Signaling Technology, 7074, 1:10000 in 5% BSA for WB); Tetrazolium chloride (Sigma-Aldrich, T-8877); NMDA (Tocris, 0114); AP5 (Cayman chemical, 14539); MK-801 (Sigma-Aldrich, M107); PMA (Sigma-Aldrich, 524400); H_2O_2 (Thermal Fisher Scientific, 200745); EGTA (Cayman chemical, 11706); BAPTA-AM (Cayman chemical, 15551); NP40 (Thermal Fisher Scientific, 28324); Triton X-100 (Thermal Fisher Scientific, T-9284), Bovine Serum Albumin (Sigma-Aldrich, 9048–46-8). All chemicals for making artificial cerebrospinal fluid (aCSF; see below) and recording solution (see below) were purchased from Sigma-Aldrich.

Membrane permeable peptide TAT-M2PBM for disrupting TRPM2 and PKCγ coupling and scramble control TAT-SC peptides—TAT-SC (sequence: YGRKKRRQRRR VILLKDHTLEYPVF), TAT-M2PBM (sequence: YGRKKRRQRRR WGLDVPNLLISVTGGA) were synthesized by GenScript Biotech and dissolved in PBS to make a stock concentration at 10 mM. HEK-293T cells or isolated neurons were treated with TAT-SC or TAT-M2PBM at a concentration of 1 μM for at least 2 h prior to use. Mice were intraperitoneal injected (i.p.) with TAT-SC or TAT-M2PBM at a dose of 100 nmol/kg. Detailed injection strategy is described in Figure 6B.

Plasmids and enzymes—GluN1a (Addgene, 17928), GluN2A (Addgene, 17924), GluN2B (Addgene, 17925), PKC-γ (Addgene, 112266), PKC-γ-DN (Addgene, 21239), CKAR (Addgene, 14860). The pcDNA4/TO-FLAG-hTRPM2 construct was a kind gift from Dr. Sharenberg AM (University of Washington, Seattle).[51] DpnI (BioLabs, R0176L) and PfuUltra HF (Agilent, 600380–51) were used to generating different deletion or mutation constructs.

Subcloning—For TRPM2, subcloning of N terminus (1–727) was achieved by introducing a stop codon (A2282T) by PCR (F: CAAGGACATGTAGTTTGTGTCTCACG, R: CGTGAGACACAAACTACATGTCCTTG) using PfuUltra HF. Mutagenesis

of S11A (F: TGAGGAAAGCTGGCGCAGAGCAGGAGGAG, R: TCCTCCTGCTCTGCGCCAGCTTTCCTCAG), S11D (F: TGAGGAAAGCTGG CGAGGAGCAGGAGGAG, R: TCCTCCTGCTCCTCGCCAGCTTTCCTCAG), S38A (F: GGCGCAGCAACGCCAGCCTCTTCAAG, R: TCTTGAAGAGGCTGGCGTTGCTGCGC), S38D (F: GGCGCAGCAACGACAGCCTCTTCAAG, R: TCTTGAAGAGGCTGTCGTTGCT GCGC) were achieved by PCR using PfuUltra HF. Deletion of the PBM were achieved by PCR (F: TACCACCTCATGA CCCAGCACAAGAACTTCAACATGAAG, R: TTCATGTTGAAGTTCTTGTGCTGGGTCATGAGGTGGTAG) using Q5 Site-Directed Mutagenesis Kit (BioLabs, E0554S) based on the manual.

PROTEIN EXPRESSION AND PURIFICATION

The C2 domain (residues 27–306) of human PKC was cloned into a modified pGEX-4T3 vector containing a removable tobacco etch virus (TEV) protease recognition site. The GST-tagged C2 domain was expressed in Escherichia coli BL21(DE3) cells grown to an OD600 (optical density at 600 nm) between 0.8 and 1.0 at 37°C followed by induction of protein expression at 21°C overnight using 0.5 mM isopropyl-D-1-thiogalactopyranoside (IPTG). Cells were harvested by centrifugation, resuspended by lysis buffer containing 25 mM Tris-HCl (pH 8.0), 200 mM NaCl, 1% phenylmethylsulfonyl fluoride (PMSF) and 2 mM dithiothreitol (DTT), and lysed by using high-pressure homogenization (Avestin EmulsiFlex C3). The lysate was clarified by centrifugation at 30,000 rpm at 4°C for 30 min, and the supernatant was applied to a Glutathione Sepharose 4B column (GE Healthcare). After being extensively washed with lysis buffer, the protein was eluted with a buffer containing 25 mM Tris-HCl (pH 8.0), 200 mM NaCl, 15 mM reduced glutathione and 2 mM DTT. The protein was further purified by size exclusion chromatography (SD200; GE Healthcare) in a buffer containing 25 mM Tris-HC (pH 8.0), 150 mM NaCl, 2 mM DTT. The protein was concentrated using an Amicon stirred ultrafiltration cell unit with a 10-kDa cutoff membrane (EMD Millipore) and stored at —80°C until use.

The MHR1/2 domain (residues 127–455) of human TRPM2 was cloned into a modified pET15b vector containing a removable TEV protease recognition site. The His6-tagged MHR1/2 domain was expressed in E. coli BL21(DE3) as described above. The cell pellet was resuspended in denaturing buffer containing 25 mM Tris-HCl (pH 8.0), 300 mM NaCl, 1% PMSF and 6 M Urea and lysed by high-pressure homogenization. The lysate was clarified by centrifugation at 30,000 rpm at 4°C for 30 min, and the supernatants were applied to a Ni^{2+}-nitrilotriacetic acid (NTA) column (GE Healthcare). After being extensively washed with 25 mM imidazole in the denaturing buffer, the protein was eluted with a buffer containing 25 mM Tris-HCl (pH 8.0), 300 mM NaCl and 250 mM imidazole. For refolding, the protein was dialyzed at 4° C overnight against two changes of a buffer without urea [25 mM Tris-HCl (pH 8.0), 200 mM NaCl and 0.1% Triton X-100]. The refolded protein was concentrated using an Amicon stirred ultrafiltration cell unit with a 10-kDa cutoff membrane and stored at —80°C until use.

Live cell imaging—CKAR experiments was performed based on a well-established protocol.[17] CKAR was transfected into HEK293T cells with other plasmids. 12 h after

transfection, cells were split onto 25 mm glass coverslips for FRET imaging. Culture medium was washed using HBSS for 3 times. Fluorescence intensities at 527 nm for YFP and 490 nm for CFP were collected at a rate of 1 Hz using CoolSNAP HQ2 (Photometrics) and data were analyzed using NIS-Elements (Nikon).

Intracellular Ca^{2+} was measured using ratio Fura2-AM imaging based on a well-established protocol.[6] In brief, Fura2-AM (Thermal Fisher Scientific, F1221) was dissolved in DMSO to make a stock concentration at 1 mM. Pre-warmed Neurobasal Medium (Thermal Fisher Scientific, 21103–049) was used to dilute Fura-2 a.m. to a working concentration at 2.5 mM, and 0.02% Pluronic F-127 (Thermal Fisher Scientific, P3000MP) was added to facilitate loading of Fura-2 a.m. Cortical neurons on 25 mm glass coverslips were washed using pre-warmed PBS for 3 times, and then incubated with 2 mL of Fura-2 a.m. working solution for 20 min at 37°C. Non-incorporated dye was washed away using HBSS. Fluorescence intensities at 510 nm with 340 nm and 380 nm excitation were collected at a rate of 1 Hz using CoolSNAP HQ2 (Photometrics) and data were analyzed using NIS-Elements (Nikon).[6]

Intracellular nitric oxide content was measured using DAF-FM imaging.[26] DAF-FM (Thermal Fisher Scientific, D23844) was dissolved in DMSO to make a stock concentration at 1 mM. Pre-warmed Neurobasal Medium was used to dilute DAF-FM to a working concentration at 1 μM for loading. Cortical neurons on 25 mm glass coverslips were washed using pre-warmed PBS for 3 times, and then incubated with 2 mL of DAF-FM working solution for 10 min at 37°C. Non-incorporated dye was washed away using HBSS. Fluorescence intensities at 515 nm was collected using CoolSNAP HQ2 and data were analyzed using NIS-Elements.

Intracellular reactive oxygen species was measured using MitoSOX imaging.[28] MitoSOX-Red (Thermal Fisher Scientific, M36008) was dissolved in DMSO to make a stock concentration at 1 mM. Pre-warmed Neurobasal Medium was used to dilute MitoSOX-Red to a working concentration at 0.5 μM for loading. Cortical neurons on 25 mm glass coverslips were washed using pre-warmed PBS for 3 times, and then incubated with 2 mL of MitoSOX-Red working solution for 15 min at room temperature. Non-incorporated dye was washed away using HBSS. Fluorescence intensities at 610 nm was collected using CoolSNAP HQ2 and data were analyzed using NIS-Elements.

Mitochondrial depolarization was evaluated using Rhodamine-123 imaging based on a well-established protocol.[6] Rhodamine-123 (Thermal Fisher Scientific, R302) dissolved in DMSO to make a stock concentration at 10 mg/mL. Pre-warmed Neurobasal Medium was used to dilute Rhodamine-123 to a working concentration at 2.5 mg/mL for loading. Cortical neurons on 25 mm glass coverslips were washed using pre-warmed PBS for 3 times, and then incubated with 2 mL of Rhodamine-123 working solution for 5 min at room temperature. Non-incorporated dye was washed away using HBSS. Fluorescence intensities at 509 nm was collected using CoolSNAP HQ2 and data were analyzed using NIS-Elements.

Mass spectrometry—Lysis buffer without NP40 (150 mM NaCl, 1 mM EDTA, 50 mM Tris, pH = 8.0) containing proteinase inhibitors (Sigma-Aldrich, 539131–10VL) and

phosphatase inhibitors (Thermal Fisher Scientific, 78428) was used to lyse HEK293T cells 24 h after transfection and 5 min after DMSO or PMA (10 μM) treatment. Cell and tissue lysate were lysed by ultrasound using an ultrasonic cleaner filled with ice-cold water for 30 min. After incubated on ice for 1 h, lysate was centrifuged at 13000 g for 30 min and supernatant was collected. Protein samples were sent for mass spectrometry analysis at UConn Proteomics & Metabolomics Center.

Co-immunoprecipitation—Co-immunoprecipitation was performed based on a well-established protocol.[6] NP-40 lysis buffer (10% NP40, 150 mM NaCl, 1 mM EDTA, 50 mM Tris, pH = 8.0) containing proteinase inhibitors (Sigma-Aldrich, 539131–10VL) and phosphatase inhibitors (Thermal Fisher Scientific, 78428) was used to lyse both cultured cells and frozen brain tissue. For transfected cells, proteins were extracted 36 h after transfection. Cell and tissue lysate were lysed by ultrasound using an ultrasonic cleaner (Thermal Fisher Scientific) filled with ice-cold water for 30 min. After incubated on ice for 1 h, lysate was centrifuged at 13000 g for 30 min and supernatant was collected. Protein concentration was measured using Pierce Rapid Gold BCA Protein Assay Kit (Thermal Fisher Scientific, A53225). 300 μg of protein was taken and diluted using NP-40 lysis buffer to make a total volume of 500 μL. Unused protein was allocated and frozen at —80°C for future use. Appropriate amount of antibody was added based on manufacturer instruction. 25 μL of pre-washed Protein A/G PLUS-Agarose (Santa Cruz Biotechnology, sc-2003) was added, and incubated at 4°C for overnight. Then the mixture was centrifuged at 2500g for 1min to get agarose beads. Agarose beads was washed using NP-40 lysis buffer for 3 times, mixed with same amount of 2x Laemmli Sample Buffer (BIO-RAD, 1610737), and boiled at 95°C for 5 min. Then samples were ready for western blotting analysis.

Western blotting—NP-40/Triton lysis buffer (10% NP40, 1% Triton X-100, 150 mM NaCl, 1 mM EDTA, 50 mM Tris, pH = 8.0) containing proteinase inhibitors and phosphatase inhibitors was used to lyse both cultured cells and frozen brain tissue. Surface protein was extracted using Pierce Cell Surface Protein Isolation Kit (Thermal Fisher Scientific, 89881) in transfected HEK-293T cells, and using ProteoExtract Native Membrane Protein Extraction Kit (Calbiochem, 444810) in brain tissue based on instructions. For transfected cells, proteins were extracted 36 h after transfection. Cell and tissue lysate were lysed by ultrasound using an ultrasonic cleaner filled with ice-cold water for 30 min. After incubated on ice for 1 h, lysate was centrifuged at 13000 g for 30 min and supernatant was collected. Protein concentration was measured using Pierce Rapid Gold BCA Protein Assay Kit.

30–50 μg of total protein was loaded and separated proteins were transferred to Nitrocellulose membranes. Membranes were blocked with 5% BSA and 2.5% goat serum in Tris-buffered saline (TBS, pH = 7.4) at room temperature for 2 h, and incubated with primary antibodies in TBS with 0.05% Tween (TBS-T) at room temperature for 2 h. Then membranes were incubated with secondary antibodies in TBS-T for 1 h at room temperature for 1 h for detection. Blots were developed with ImageQuant LAS 4000 imaging system. Band intensity was quantified using ImageJ software[43] and normalized with appropriate loading controls.

Electrophysiology—Whole cell currents were recorded using an Axopatch 200B amplifier. Data were digitized at 10 or 20 kHz and digitally filtered offline at 1 kHz. Patch electrodes were pulled from borosilicate glass and fire-polished to a resistance of ~3 MΩ when filled with internal solutions. Series resistance (R_s) was compensated up to 90% to reduce series resistance errors to <5 mV. Cells in which R_s was >10 MΩ were discarded.[52]

For heterologous expression, transfected HEK-293 cells were identified by GFP fluorescence. TRPM2 current recording in transfected HEK-293T cells was performed as we previously reported.[6] TRPM2 and NMDAR currents recordings from cultured neurons were performed using aCSF as extracellular solution as we previously reported.[6] In brief, for TRPM2 current recordings, voltage stimuli lasting 250 ms were delivered at 1-s intervals, with voltage ramps ranging from —100 to +100 mV at holding potential of 0 mV to elicited currents. For NMDAR current recordings, a gap-free protocol at holding potential of —80 mV was applied to elicit NMDA currents upon agonist stimulation. A fast perfusion system was used to exchange extracellular solutions and to deliver agonists and antagonists to the cells, with a complete solution exchange achieved in about 1–3 s.[53]

Normal Tyrode solution for current recording in HEK-293 cells contained (mM): 145 NaCl, 5 KCl, 2 $CaCl_2$, 10 HEPES, 10 glucose, osmolarity = 290–320 mOsm/Kg, and pH = 7.4 was adjusted with NaOH. Extracellular solution for current recording in neuron, the aCSF solution contained (mM):124 NaCl, 2.5 KCl, 2 $MgSO_4$, 2 $CaCl_2$, 1.2 NaH_2PO_4, 24 $NaHCO_3$, 5 HEPES, 12.5 glucose, osmolarity = 300–310 mOsm/Kg, with pH = 7.4 adjusted with NaOH. For oxygen-glucose-deprivation (OGD) solution, glucose was eliminated from extracellular solution, and the solution was saturated with nitrogen (N_2) bubbling for 30 min before the experiments.

The internal pipette solution for whole cell current recordings of TRPM2 overexpressed in HEK293 cells contained (in mM): 135 Cs-methanesulfonate ($CsSO_3CH_3$), 8 NaCl, 0.5 $CaCl_2$, 1 EGTA, and 10 HEPES, with pH adjusted to 7.2 with CsOH. Free $[Ca^{2+}]_i$ buffered by EGTA was ~100 nM calculated using Max chelator.[52] ADPR 1 μM was included in the pipette solution for the minimal basal activation of TRPM2. Ca^{2+} concentration was increased to 1 mM and EGTA was removed, while ADPR concentration was increased to 500 μM to achieve the maximal activation of TRPM2 current. The intracellular solution for NMDAR current recording contained (mM): 110 K-ASP, 20 KCl, 1 $MgSO_4$, 10 mM BAPTA, 0.1 GTP, 5 ATP-Mg_2, 10 HEPES, osmolarity = 275–285 mOsm/Kg, pH = 7.2 adjusted with KOH. For the experiments using cells pretreated with the disrupting peptides TAT-SC and TAT-M2PBM, 1 μM TAT-SC or TAT-M2PBM was included in the pipette solution, and at least 10 min was allowed for achieving intracellular equilibration of TAT-SC or TAT-EE_3 before current recording. For current recordings in neurons, tetrodotoxin (0.5 μM) was included in the external solution to block voltage-gated Na^+ current, and 10 μM nifedipine was used to block voltage-gated Ca^{2+} currents for recording TRPM2 currents.

The above-mentioned pipette solutions and extracellular solutions were specific for TRPM2 or NMDAR current recordings, without “cross-contamination” for each other or from other channel activation. The omitting of ADPR and including high concentration of potent calcium chelator BAPTA in the pipette solution for NMDAR current recordings eliminated

any possibility of TRPM2 channel activation because TRPM2 requires Ca^{2+} and ADPR to be activated. Ca^{2+}-free pipette solution for NMDAR current recording also prevented other Ca^{2+}-activated currents such as TRPM4. Moreover, using $CsSO_3CH_3$ in the pipette solution for TRPM2 current recordings eliminated contamination from any potassium channels for recordings in neurons and in HEK-293 cells.

QUANTIFICATION AND STATISTICAL ANALYSIS

All data are expressed as mean ± standard error of the mean (SEM) and "n" is the number of biological replicates. Experiments were repeated at least three times. Sample size was estimated by Power analysis using the webtool7 (https://clincalc.com/stats/samplesize.aspx), or G*Power software8 (http://www.gpower.hhu.de/), which utilize independent study groups, type I error $\alpha = 0.05$ and power = 80%. Randomization was used to divide animals or experimental samples into separated groups that compare different treatments to avoid bias in all our experiments. Random assignment subjects to different treatment groups were performed using GraphPad "Random number calculators" to assign subjects to different groups. GraphPad Prism v9 (GraphPad Software, Inc.) was also used for statistical analyses. Data quantification and analysis were performed blindly. Prior to statistical analysis, data were analyzed for normality by Kolmogorov-Smirnov test or Shapiro-Wilk test as a justification for using Student's t-test or analysis of variance (ANOVA). Equal variance was analyzed using Bartlett test and F-test for multiple comparison groups and two-sample t test respectively. If normality and equal variance were not satisfied, Mann-Whitney test was used for statistical analysis for two groups' comparison and Kruskal-Wallis non-parametric test, with Dun's multiple comparison, was used for comparison between multiple groups as previously reported7. In GraphPad Prism 9.0, Welch's ANOVA and Brown-Forsythe ANOVA also automatically adjusts the calculations of the F ratio and degrees of freedom to adjust for heterogeneity of within-group variances. The *p* value can be interpreted in the same manner as in the analysis of variance. For two groups' comparison, statistical significance was determined using two-tailed Student's t-test. For multiple groups, statistical significance was determined using one-way or two-way ANOVA, followed by Bonferroni post-test with correction. One-way ANOVA was used for comparison of multiple groups with one variable, and two-way ANOVA was used when there were two independent variables. Two-sided $p < 0.05$ was considered as significant. The details of statistical analysis can be found in the figure legends (such as t test or ANOVA for analysis, and indicators of *p* values (ns, no statistical significance, *, $p < 0.05$, **, $p < 0.01$, ***, $p < 0.001$)). The sample size for Western blot experiments means six dishes of cells from at least two mice. The sample size for live cell imaging experiments means 20–40 cells from at least three dishes of cells, which were collected from more than two mice. The exact value of n can be found in the figure legends.

Supplementary Material

Refer to Web version on PubMed Central for supplementary material.

ACKNOWLEDGMENTS

We would like to thank Dr. Rajkumar Verma (UCONN Health) and Dr. Louise McCullough (UT Health) for constructive discussions about this project. We thank Dr. Andrew M. Scharenberg (University of Washington) for kindly providing the TRPM2 plasmid. This work was partially supported by the National Institutes of Health (R01-HL143750 and R01NS131661) and the American Heart Association (19TPA34890022) to L.Y. and by the Connecticut Institute for the Brain and Cognitive Sciences Seed Grant (402194) to P.Z.

REFERENCES

1. Campbell BCV, De Silva DA, Macleod MR, Coutts SB, Schwamm LH, Davis SM, and Donnan GA (2019). Ischaemic stroke. Nat. Rev. Dis. Primers 5, 70. 10.1038/s41572-019-0118-8. [PubMed: 31601801]
2. Watkins JC, and Jane DE (2006). The glutamate story. Br. J. Pharmacol 147, S100–S108. 10.1038/sj.bjp.0706444. [PubMed: 16402093]
3. Wu QJ, and Tymianski M. (2018). Targeting NMDA receptors in stroke: new hope in neuroprotection. Mol. Brain 11, 15. 10.1186/s13041-018-0357-8. [PubMed: 29534733]
4. Petit-Pedrol M, and Groc L. (2021). Regulation of membrane NMDA receptors by dynamics and protein interactions. J. Cell Biol. 220, e202006101. 10.1083/jcb.202006101.
5. Yan J, Bengtson CP, Buchthal B, Hagenston AM, and Bading H. (2020). Coupling of NMDA receptors and TRPM4 guides discovery of unconventional neuroprotectants. Science 370, eaay3302. 10.1126/science.aay3302.
6. Zong P, Feng J, Yue Z, Li Y, Wu G, Sun B, He Y, Miller B, Yu AS, Su Z, et al. (2022). Functional coupling of TRPM2 and extrasynaptic NMDARs exacerbates excitotoxicity in ischemic brain injury. Neuron 110, 1944–1958.e8. 10.1016/j.neuron.2022.03.021. [PubMed: 35421327]
7. Zong P, Lin Q, Feng J, and Yue L. (2022). A Systemic Review of the Integral Role of TRPM2 in Ischemic Stroke: From Upstream Risk Factors to Ultimate Neuronal Death. Cells 11, 491. 10.3390/cells11030491. [PubMed: 35159300]
8. Zong P, Feng J, Yue Z, Yu AS, Vacher J, Jellison ER, Miller B, Mori Y, and Yue L. (2022). TRPM2 deficiency in mice protects against atherosclerosis by inhibiting TRPM2-CD36 inflammatory axis in macrophages. Nat. Cardiovasc. Res 1, 344–360. 10.1038/s44161-022-00027-7. [PubMed: 35445217]
9. Bright R, and Mochly-Rosen D. (2005). The role of protein kinase C in cerebral ischemic and reperfusion injury. Stroke 36, 2781–2790. 10.1161/01.STR.0000189996.71237.f7. [PubMed: 16254221]
10. Callender JA, and Newton AC (2017). Conventional protein kinase C in the brain: 40 years later. Neuronal Signal. 1, NS20160005. 10.1042/NS20160005.
11. Lan JY, Skeberdis VA, Jover T, Grooms SY, Lin Y, Araneda RC, Zheng X, Bennett MV, and Zukin RS (2001). Protein kinase C modulates NMDA receptor trafficking and gating. Nat. Neurosci 4, 382–390. 10.1038/86028. [PubMed: 11276228]
12. Newton AC (2018). Protein kinase C: perfectly balanced. Crit. Rev. Bio-chem. Mol. Biol 53, 208–230. 10.1080/10409238.2018.1442408.
13. Gada KD, and Logothetis DE (2022). PKC regulation of ion channels: The involvement of PIP(2). J. Biol. Chem 298, 102035. 10.1016/j.jbc.2022.102035.
14. Kang JH, Toita R, Kim CW, and Katayama Y. (2012). Protein kinase C (PKC) isozyme-specific substrates and their design. Biotechnol. Adv 30, 1662–1672. 10.1016/j.biotechadv.2012.07.004. [PubMed: 22841933]
15. Newton AC (1997). Regulation of protein kinase C. Curr. Opin. Cell Biol. 9, 161–167. 10.1016/s0955-0674(97)80058-0. [PubMed: 9069266]
16. Sumoza-Toledo A, and Penner R. (2011). TRPM2: a multifunctional ion channel for calcium signalling. J. Physiol 589, 1515–1525. 10.1113/jphysiol.2010.201855. [PubMed: 21135052]
17. Violin JD, Zhang J, Tsien RY, and Newton AC (2003). A genetically encoded fluorescent reporter reveals oscillatory phosphorylation by protein kinase C. J. Cell Biol. 161, 899–909. 10.1083/jcb.200302125. [PubMed: 12782683]

18. Kraft R, Grimm C, Frenzel H, and Harteneck C. (2006). Inhibition of TRPM2 cation channels by N-(p-amylcinnamoyl)anthranilic acid. Br. J. Pharmacol 148, 264–273. 10.1038/sj.bjp.0706739. [PubMed: 16604090]
19. Schwaller B. (2010). Cytosolic Ca2+ buffers. Cold Spring Harb. Perspect. Biol 2, a004051. 10.1101/cshperspect.a004051.
20. Ron D, and Mochly-Rosen D. (1994). Agonists and antagonists of protein kinase C function, derived from its binding proteins. J. Biol. Chem 269, 21395–21398. [PubMed: 8063768]
21. Adams DR, Ron D, and Kiely PA (2011). RACK1, A multifaceted scaffolding protein: Structure and function. Cell Commun. Signal 9, 22. 10.1186/1478-811X-9-22. [PubMed: 21978545]
22. Weilinger NL, Lohman AW, Rakai BD, Ma EMM, Bialecki J, Maslieieva V, Rilea T, Bandet MV, Ikuta NT, Scott L, et al. (2016). Metabotropic NMDA receptor signaling couples Src family kinases to pannexin-1 during excitotoxicity. Nat. Neurosci 19, 432–442. 10.1038/nn.4236. [PubMed: 26854804]
23. Tasca CI, Dal-Cim T, and Cimarosti H. (2015). In vitro oxygen-glucose deprivation to study ischemic cell death. Methods Mol. Biol 1254, 197–210. 10.1007/978-1-4939-2152-2_15.
24. Kristián T, and Siesjö BK (1998). Calcium in ischemic cell death. Stroke 29, 705–718. 10.1161/01.str.29.3.705. [PubMed: 9506616]
25. Brown GC (2010). Nitric oxide and neuronal death. Nitric Oxide 23, 153–165. 10.1016/j.niox.2010.06.001. [PubMed: 20547235]
26. Tjalkens RB, Carbone DL, and Wu G. (2011). Detection of nitric oxide formation in primary neural cells and tissues. Methods Mol. Biol 758, 267–277. 10.1007/978-1-61779-170-3_18. [PubMed: 21815072]
27. Dixon SJ, and Stockwell BR (2014). The role of iron and reactive oxygen species in cell death. Nat. Chem. Biol 10, 9–17. 10.1038/nchembio.1416. [PubMed: 24346035]
28. Fernandez A, Meechan DW, Karpinski BA, Paronett EM, Bryan CA, Rutz HL, Radin EA, Lubin N, Bonner ER, Popratiloff A, et al. (2019). Mitochondrial Dysfunction Leads to Cortical Under-Connectivity and Cognitive Impairment. Neuron 102, 1127–1142.e3. 10.1016/j.neuron.2019.04.013. [PubMed: 31079872]
29. Norat P, Soldozy S, Sokolowski JD, Gorick CM, Kumar JS, Chae Y, Yağmurlu K, Prada F, Walker M, Levitt MR, et al. (2020). Mitochondrial dysfunction in neurological disorders: Exploring mitochondrial transplantation. NPJ Regen. Med 5, 22. 10.1038/s41536-020-00107-x.
30. Scaduto RC Jr., and Grotyohann LW (1999). Measurement of mitochondrial membrane potential using fluorescent rhodamine derivatives. Biophys. J 76, 469–477. 10.1016/S0006-3495(99)77214-0. [PubMed: 9876159]
31. Kristensen M, Birch D, and Mørck Nielsen H. (2016). Applications and Challenges for Use of Cell-Penetrating Peptides as Delivery Vectors for Peptide and Protein Cargos. Int. J. Mol. Sci 17, 185. 10.3390/ijms17020185. [PubMed: 26840305]
32. Zhang W, Tong Q, Conrad K, Wozney J, Cheung JY, and Miller BA (2007). Regulation of TRP channel TRPM2 by the tyrosine phosphatase PTPL1. Am. J. Physiol. Cell Physiol. 292, C1746–C1758. 10.1152/ajpcell.00569.2006. [PubMed: 17251321]
33. Hecquet CM, Zhang M, Mittal M, Vogel SM, Di A, Gao X, Bonini MG, and Malik AB (2014). Cooperative interaction of trp melastatin channel transient receptor potential (TRPM2) with its splice variant TRPM2 short variant is essential for endothelial cell apoptosis. Circ. Res 114, 469–479. 10.1161/CIRCRESAHA.114.302414. [PubMed: 24337049]
34. Kashio M, Masubuchi S, and Tominaga M. (2022). Protein kinase C-mediated phosphorylation of transient receptor potential melastatin type 2 Thr738 counteracts the effect of cytosolic Ca(2+) and elevates the temperature threshold. J. Physiol 600, 4287–4302. 10.1113/JP283350. [PubMed: 36042566]
35. Verma S, Quillinan N, Yang YF, Nakayama S, Cheng J, Kelley MH, and Herson PS (2012). TRPM2 channel activation following in vitro ischemia contributes to male hippocampal cell death. Neurosci. Lett 530, 41–46. 10.1016/j.neulet.2012.09.044. [PubMed: 23041043]
36. Xie J, Bi Y, Zhang H, Dong S, Teng L, Lee RJ, and Yang Z. (2020). Cell-Penetrating Peptides in Diagnosis and Treatment of Human Diseases: From Preclinical Research to Clinical Application. Front. Pharmacol 11, 697. 10.3389/fphar.2020.00697. [PubMed: 32508641]

37. Wu Y, Luo X, Liu X, Liu D, Wang X, Guo Z, Zhu L, Tian Q, Yang X, and Wang JZ (2015). Intraperitoneal Administration of a Novel TAT-BDNF Peptide Ameliorates Cognitive Impairments via Modulating Multiple Pathways in Two Alzheimer's Rodent Models. Sci. Rep 5, 15032. 10.1038/srep15032. [PubMed: 26463268]
38. Palm-Apergi C, Lönn P, and Dowdy SF (2012). Do cell-penetrating peptides actually "penetrate" cellular membranes? Mol. Ther 20, 695–697. 10.1038/mt.2012.40. [PubMed: 22472979]
39. Carter E, Lau CY, Tosh D, Ward SG, and Mrsny RJ (2013). Cell penetrating peptides fail to induce an innate immune response in epithelial cells in vitro: implications for continued therapeutic use. Eur. J. Pharm. Biopharm 85, 12–19. 10.1016/j.ejpb.2013.03.024. [PubMed: 23958314]
40. Luo JH, Fu ZY, Losi G, Kim BG, Prybylowski K, Vissel B, and Vicini S. (2002). Functional expression of distinct NMDA channel subunits tagged with green fluorescent protein in hippocampal neurons in culture. Neuropharmacology 42, 306–318. 10.1016/s0028-3908(01)00188-5. [PubMed: 11897109]
41. Soh JW, and Weinstein IB (2003). Roles of specific isoforms of protein kinase C in the transcriptional control of cyclin D1 and related genes. J. Biol. Chem 278, 34709–34716. 10.1074/jbc.M302016200. [PubMed: 12794082]
42. Oancea E, Teruel MN, Quest AF, and Meyer T. (1998). Green fluorescent protein (GFP)-tagged cysteine-rich domains from protein kinase C as fluorescent indicators for diacylglycerol signaling in living cells. J. Cell Biol. 140, 485–498. 10.1083/jcb.140.3.485. [PubMed: 9456311]
43. Schneider CA, Rasband WS, and Eliceiri KW (2012). NIH Image to ImageJ: 25 years of image analysis. Nat. Methods 9, 671–675. 10.1038/nmeth.2089. [PubMed: 22930834]
44. Yamamoto S, Shimizu S, Kiyonaka S, Takahashi N, Wajima T, Hara Y, Negoro T, Hiroi T, Kiuchi Y, Okada T, et al. (2008). TRPM2-mediated Ca2+influx induces chemokine production in monocytes that aggravates inflammatory neutrophil infiltration. Nat. Med 14, 738–747. 10.1038/nm1758. [PubMed: 18542050]
45. Liu F, and McCullough LD (2014). The middle cerebral artery occlusion model of transient focal cerebral ischemia. Methods Mol. Biol 1135, 81–93. 10.1007/978-1-4939-0320-7_7. [PubMed: 24510856]
46. Wu LJ, Wu G, Akhavan Sharif MR, Baker A, Jia Y, Fahey FH, Luo HR, Feener EP, and Clapham DE (2012). The voltage-gated proton channel Hv1 enhances brain damage from ischemic stroke. Nat. Neurosci 15, 565–573. 10.1038/nn.3059. [PubMed: 22388960]
47. Chiang T, Messing RO, and Chou WH (2011). Mouse model of middle cerebral artery occlusion. J. Vis. Exp, e2761. 10.3791/2761.
48. Longa EZ, Weinstein PR, Carlson S, and Cummins R. (1989). Reversible middle cerebral artery occlusion without craniectomy in rats. Stroke 20, 84–91. [PubMed: 2643202]
49. Schulien AJ, Yeh CY, Orange BN, Pav OJ, Hopkins MP, Moutal A, Khanna R, Sun D, Justice JA, and Aizenman E. (2020). Targeted disruption of Kv2.1-VAPA association provides neuroprotection against ischemic stroke in mice by declustering Kv2.1 channels. Sci. Adv 6, eaaz8110. 10.1126/sciadv.aaz8110.
50. Ren M, Senatorov VV, Chen RW, and Chuang DM (2003). Postinsult treatment with lithium reduces brain damage and facilitates neurological recovery in a rat ischemia/reperfusion model. Proc. Natl. Acad. Sci. USA 100, 6210–6215. 10.1073/pnas.0937423100. [PubMed: 12732732]
51. Perraud AL, Schmitz C, and Scharenberg AM (2003). TRPM2 Ca2+ permeable cation channels: from gene to biological function. Cell Calcium 33, 519–531. [PubMed: 12765697]
52. Du J, Xie J, and Yue L. (2009). Modulation of TRPM2 by acidic pH and the underlying mechanisms for pH sensitivity. J. Gen. Physiol 134, 471–488. 10.1085/jgp.200910254. [PubMed: 19917732]
53. Jiang J, Li M, and Yue L. (2005). Potentiation of TRPM7 inward currents by protons. J. Gen. Physiol 126, 137–150. [PubMed: 16009728]

Highlights

- TRPM2's PBM directly binds to PKCγ's C2 domain
- TRPM2-PKCγ binding promotes the activation of each other
- TRPM2-PKCγ coupling enhances ischemic excitotoxicity
- Uncoupling TRPM2-PKCγ interaction by TAT-M2PMB mitigates ischemic brain injury

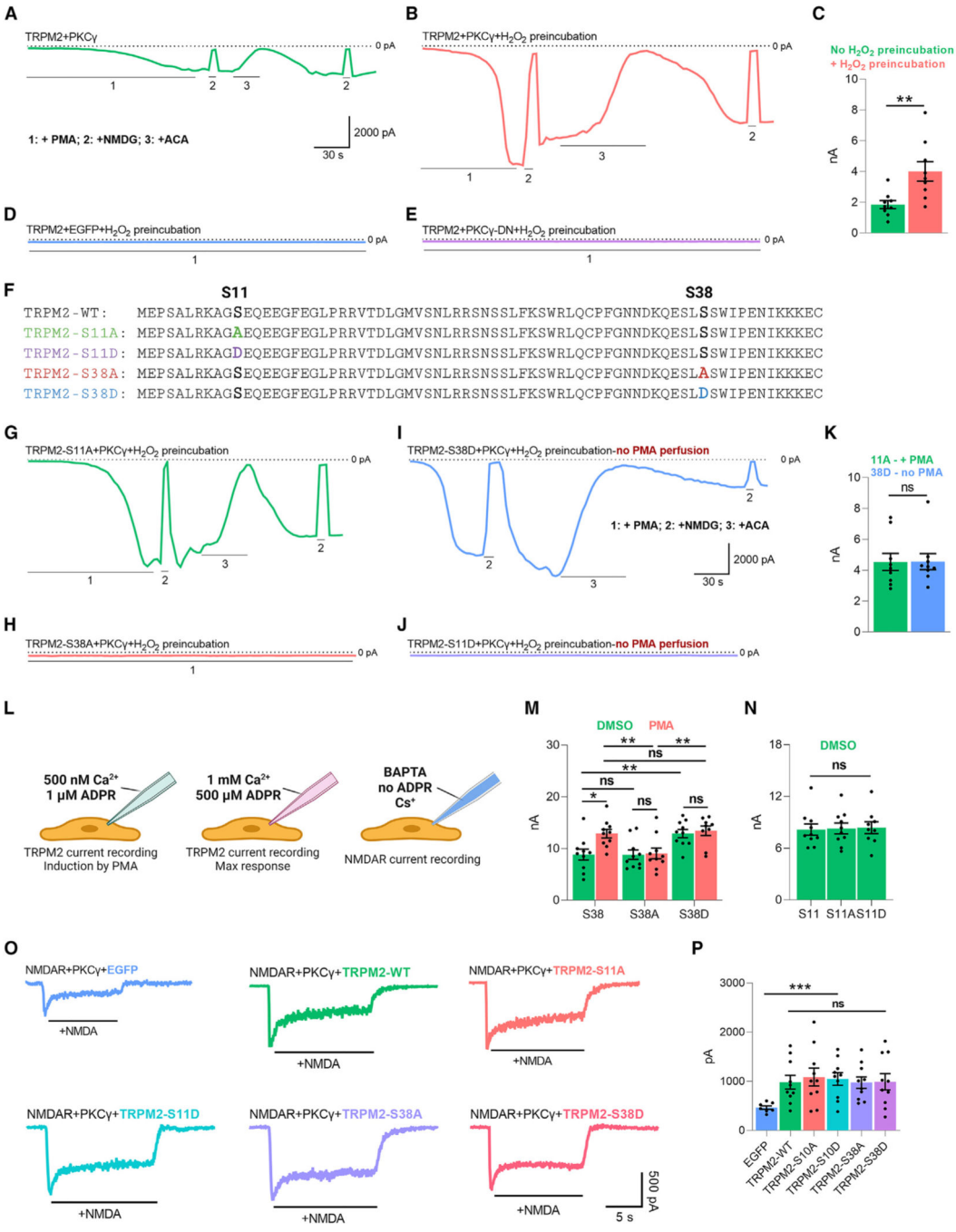

Figure 1. PKCγ phosphorylates TRPM2 and enhances TRPM2 activation

(A–C) Whole-cell current recording of TRPM2 in HEK293T cells transfected with TRPM2/PKCγ without (A) or with (B) H_2O_2 preincubation for 3 min.

(A and B) Time-dependent activation of TRPM2 as indicated by the inward currents plotted against time. TRPM2 currents were elicited by a ramp protocol with pipette solution containing 1 μM ADPR and 500 nM Ca^{2+}. PMA (10 μM) was used to induce TRPM2 activation, NMDG to test seal tightness, and anthranilic acid (ACA) to block TRPM2 current.

(C) Quantification of current amplitude (n = 9, 9).
(D and E) Whole-cell current recording of TRPM2 in HEK293T cells transfected with TRPM2/GFP (D) and TRPM2/PKCγ-DN (E).
(F) Mutation of S11 to S11A/D and S38 to S38A/D.
(G–K) Whole-cell current recording of TRPM2 in HEK293T cells transfected with TRPM2-S11A/PKCγ (G), TRPM2-S38A/PKCγ (H), TRPM2-S38D/PKCγ (I), and TRPM2-S11D/PKCγ (J).
(G–J) Representative traces.
(K) Quantification of current amplitude (n = 9, 9).
(L) Internal solution for recording TRPM2 and NMDAR currents.
(M) Quantification of TRPM2 current amplitude under maximum activation recording conditions (S38: TRPM2-WT; S38A: TRPM2-S38A; S38D: TRPM2-S38D) (n = 10, 10, 10, 10, 11, 8).
(N) Quantification of TRPM2 current amplitude under maximum activation recording conditions (S11: TRPM2-WT; S11A: TRPM2-S11A; S11D: TRPM2-S11D) (n = 9, 10, 9).
(O and P) Whole-cell current recordings of NMDARs induced by 100 μM NMDA in HEK293T cells transfected with NMDAR/PKCγ and EGFP control, TRPM2-WT, TRPM2-S11A, TRPM2-S11D, TRPM2-S38A, and TRPM2-S38D (O) and quantification of current amplitude (P) (n = 7, 11, 10, 10, 9, 10).
ns, no statistical significance, *p < 0.05, **p < 0.01, ***p < 0.001; unpaired t test; mean ± SEM.

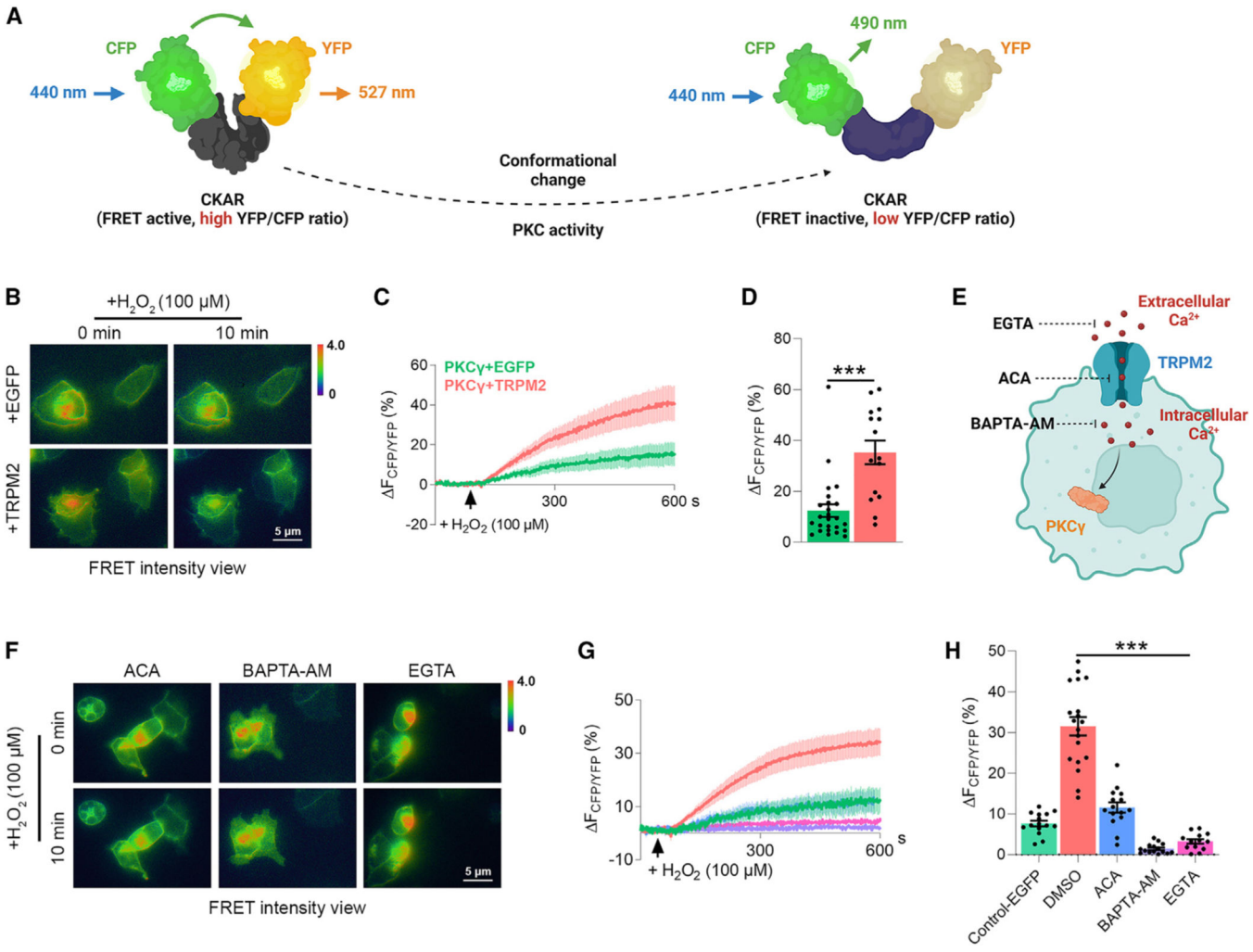

Figure 2. TRPM2-mediated Ca^{2+} influx promotes PKCγ activation

(A) FRET sensor CKAR consists of a CFP, a YFP, and a linker. Without PKC activity, CFP and YFP are in close proximity (<10 nm) for FRET (emission of CFP by 440 nm excitation excites YFP and yields a 527 emission). PKC phosphorylates CKAR, which changes the conformation of the linker and eliminates FRET (490 nm emission of CFP cannot excite YFP).

(B–D) CKAR real-time imaging in HEK293T cells transfected with TRPM2/PKCγ and EGFP/PKCγ.

(B) FRET intensity view before and 10 min after 100 μM H_2O_2 perfusion.

(C) Averaged representative traces from 5 randomly chosen cells.

(D) Quantification of FRET changes (n = 10–20).

(E) Graphic illustration showing where EGTA, ACA, and BAPTA-AM target.

(F–H) CKAR real-time imaging in HEK293T cells transfected with TRPM2/PKCγ pretreated with ACA (10 μM) or BAPTA-AM (10 μM) for 30 min and perfused with Ca^{2+} free extracellular solution buffered by 2 mM EGTA.

(F) FRET intensity before and 10 min after 100 μM H_2O_2 perfusion.

(G) Averaged representative traces from 5 randomly chosen cells.

(H) Quantification of FRET changes (n = 10–20).

***p < 0.001; unpaired t test; mean ± SEM; scale bar: 5 μm.

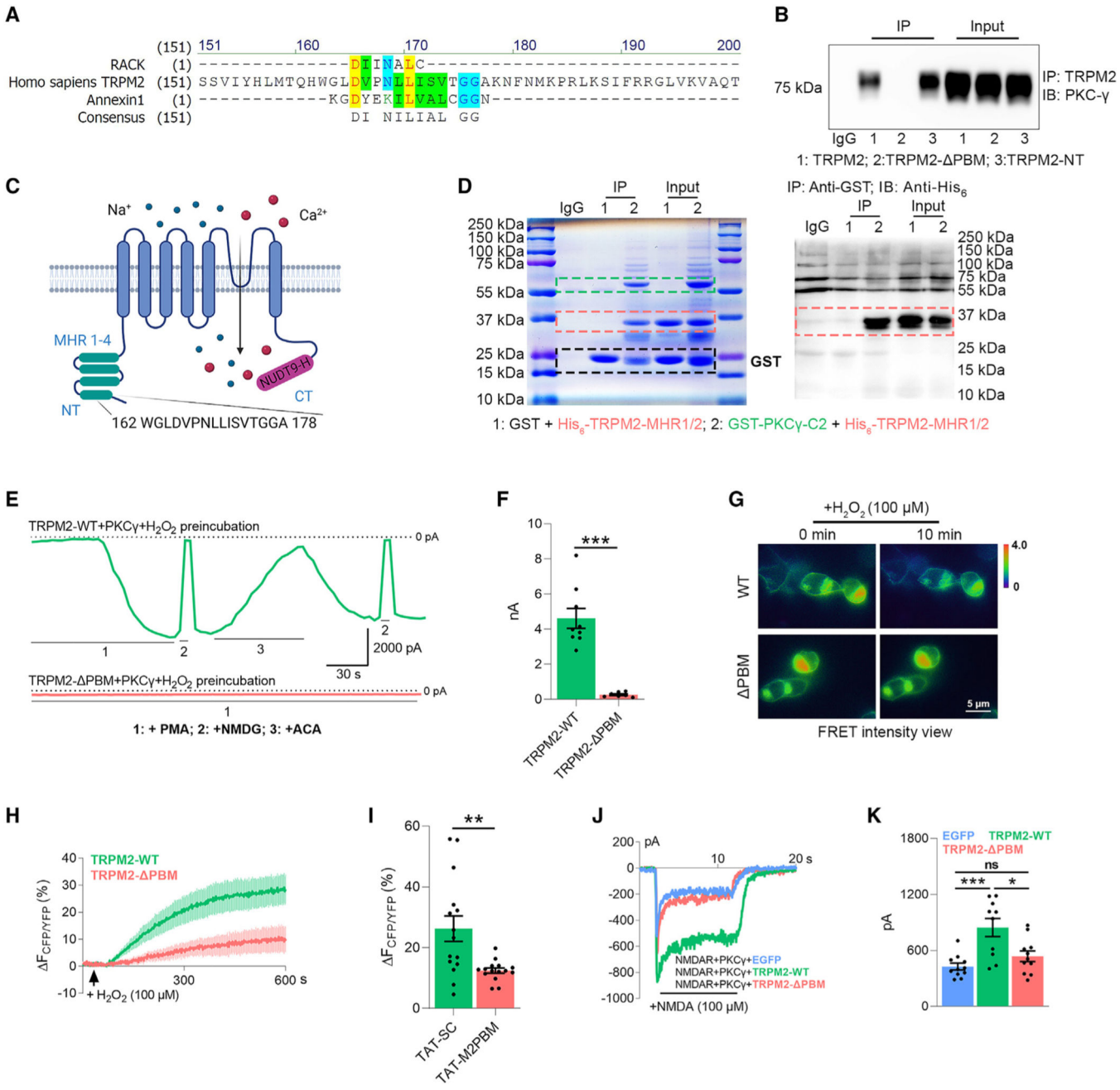

Figure 3. PKCγ binding motif in TRPM2 is required for TRPM2-PKCγ coupling

(A) Alignment of the PKC binding sequence in RACK and annexin1 with human TRPM2.

(B) Co-immunoprecipitation of PKCγ by TRPM2 in HEK293T cells co-expressed with PKCγ and TRPM2, N tail of TRPM2 (TRPM2-NT), and PKC-binding-motifdeleted TRPM2 (TRPM2-DPBM).

(C) Graphic illustration showing the structure of TRPM2 and the position of PBM.

(D) *In vitro* binding assay. The C2 domain of PKCγ was conjugated with a GST tag, while the MHR1/2 domain of TRPM2 was conjugated with a His_6 tag. Anti-GST antibody was used for immunoprecipitation, and GST was used as a negative control (labeled as #2). Pull-

down efficiency was evaluated using Coomassie blue staining (left) and immunoblotting by anti-His_6 antibody (right).

(E and F) Whole-cell current recording of TRPM2 in HEK293T cells transfected with PKCγ and TRPM2-WT (green) or TRPM2-ΔPBM (red).

(E) Representative traces. PMA (10 μM) was used to induce TRPM2 activation, NMDG to test seal tightness, and ACA to block TRPM2 current.

(F) Quantification of current amplitude (n = 9, 8).

(G–I) CKAR real-time imaging in HEK293T cells transfected with PKCγ and TRPM2-WT (green) or TRPM2-ΔPBM (red).

(G) FRET intensity before and 10 min after 100 μM H_2O_2 perfusion.

(H) Averaged representative traces from 5 randomly chosen cells.

(I) Quantification of FRET changes (n = 10–20).

(J and K) Whole-cell current recording of NMDAR in HEK293T cells transfected with NMDAR/PKCγ and EGFP control (blue), TRPM2-WT (green), and TRPM2-ΔPBM (red).

(J) Representative traces of NMDARs elicited by 100 μM NMDA.

(K) Quantification of current amplitude (n = 9, 10, 11).

ns, no statistical significance, *p < 0.05, **p < 0.01, ***p < 0.001; unpaired t test; mean ± SEM; scale bar: 5 μm.

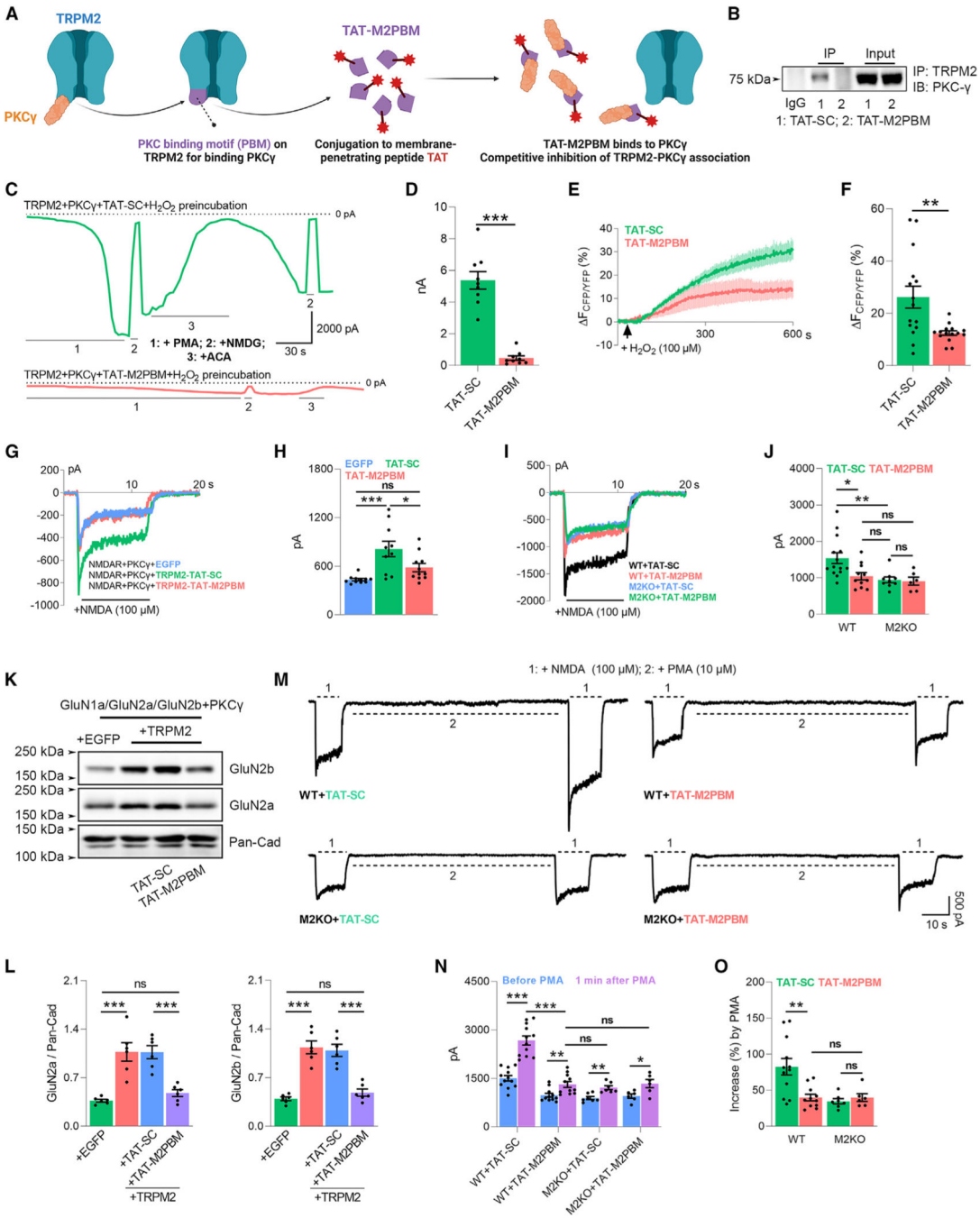

Figure 4. Disruption of TRPM2-PKCγ coupling by TAT-M2PBM

(A) Graphic illustration showing how TAT-M2PBM works. The PKCγ binding motif of TRPM2 (M2PBM) in conjugation with the cell-penetrating peptide TAT was synthesized. TAT-M2PBM binds to the TRPM2 binding site for PKCγ, thus achieving the competitive inhibition on the binding of TRPM2 to PKCγ.

(B) Co-immunoprecipitation of PKCγ by TRPM2 in HEK293T cells co-expressed with PKCγ and TRPM2 treated with TAT-SC (scramble) or TAT-M2PBM at 1 μM for 2 h.

(C and D) Whole-cell current recording of TRPM2 in HEK293T cells transfected with PKCγ and TRPM2 treated with TAT-SC (green) or TAT-M2PBM (red).
(C) Representative traces. PMA (10 μM) was used to induce TRPM2 activation, NMDG to test seal tightness, and ACA to block TRPM2 current.
(D) Quantification of current amplitude (n = 9, 9).
(E and F) CKAR real-time imaging in HEK293T cells transfected with PKCγ and TRPM2 treated with TAT-SC (green) or TAT-M2PBM (red).
(E) Averaged representative traces from 5 randomly chosen cells.
(F) Quantification of FRET changes (n = 10–20).
(G and H) Whole-cell current recording of NMDARs in HEK293T cells transfected with NMDARs/PKCγ and TRPM2 treated with TAT-SC (green) or TAT-M2PBM (red).
(G) Representative traces. NMDA (100 μM) was used to induce NMDAR activation.
(H) Quantification of current amplitude (n = 11, 10, 11).
(I and J) Whole-cell current recording of NMDARs in neurons isolated from the WT and M2KO mice treated with TAT-SC or TAT-M2PBM.
(I) Representative traces.
(J) Quantification of current amplitude (n = 15, 11, 9, 6).
(K and L) Surface expression of GluN2a and GluN2b in HEK293T cells transfected with NMDAR/PKCγ and TRPM2 treated with TAT-SC or TAT-M2PBM.
(K) Representative western blot (WB) bands.
(L) Quantification of relative expression normalized to pan-cadherin (n = 6/group).
(M–O) Whole-cell current recording of NMDARs in neurons isolated from the WT and M2KO mice treated with TAT-SC or TAT-M2PBM.
(M) Representative traces. PMA at 10 μM was used to enhance NMDAR's activity for 60 s.
(N) Quantification of current amplitude before and after PMA perfusion.
(O) Quantification of current increases after PMA perfusion (n = 6–10/group).
ns, no statistical significance, *$p < 0.05$, **$p < 0.01$, ***$p < 0.001$; unpaired t test; mean ± SEM.

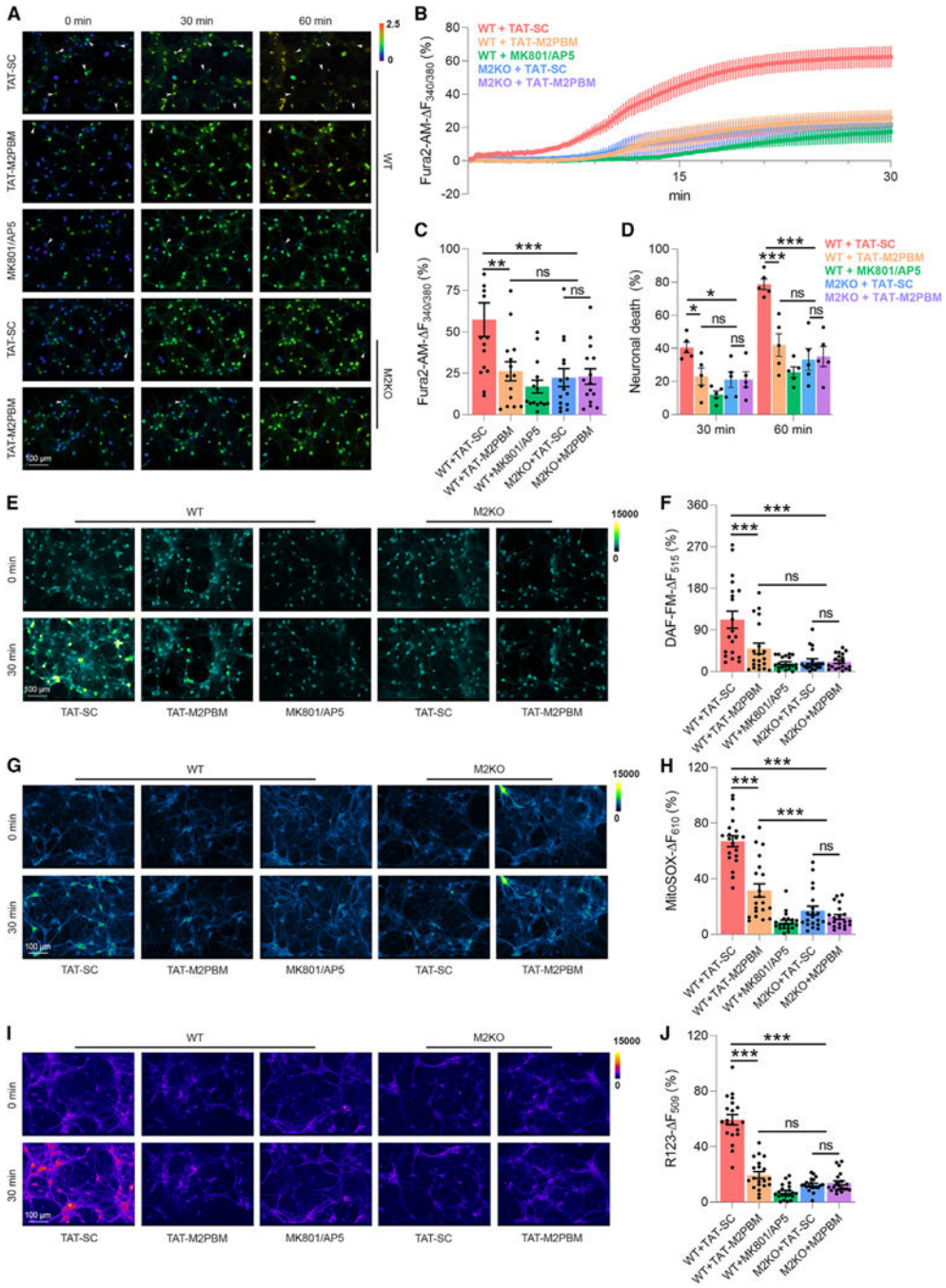

Figure 5. TAT-M2PBM attenuates ischemic neuronal death *in vitro*

(A–D) Ratio Ca^{2+} imaging of neurons isolated from WT and *Trpm2* deletion (M2KO) mice subjected to OGD. Neurons were treated with MK801/AP5 (10 μM), TAT-SC (1 μM), or TAT-M2PBM (1 μM).

(A) Representative images showing Ca^{2+} overload and neuronal death (indicated by white arrows).

(B) Averaged traces from 10 randomly chosen neurons.

(C) Quantification of Ca^{2+} increases 30 min after OGD (n = 10–20/group).

(D) Quantification of neuronal death at 30 and 60 min of OGD (n = 5/group).
(E and F) DAF-FM nitric oxide (NO) imaging of neurons isolated from WT and M2KO mice subjected to OGD. Neurons were treated with MK801/AP5, TAT-SC, or TAT-M2PBM.
(E) Representative images showing NO production.
(F) Quantification of NO increase 30 min after OGD (n = 10–20/group).
(G and H) MitoSOX reactive oxygen species (ROS) imaging of neurons isolated from WT and M2KO mice subjected to OGD. Neurons were treated with MK801/AP5, TAT-SC, or TAT-M2PBM.
(G) Representative images showing ROS generation.
(H) Quantification of ROS increase 30 min after OGD (n = 10–20/group).
(I and J) Rhodamine 123 (R123) mitochondrial membrane potential imaging of neurons isolated from WT and M2KO mice subjected to OGD. Neurons were treated with MK801/AP5, TAT-SC, or TAT-M2PBM.
(G) Representative images showing mitochondrial depolarization.
(H) Quantification of R123 increase 30 min after OGD (n = 10–20/group).
ns, no statistical significance, *$p < 0.05$, **$p < 0.01$, ***$p < 0.001$; unpaired t test; mean ± SEM; scale bar: 100 μm)

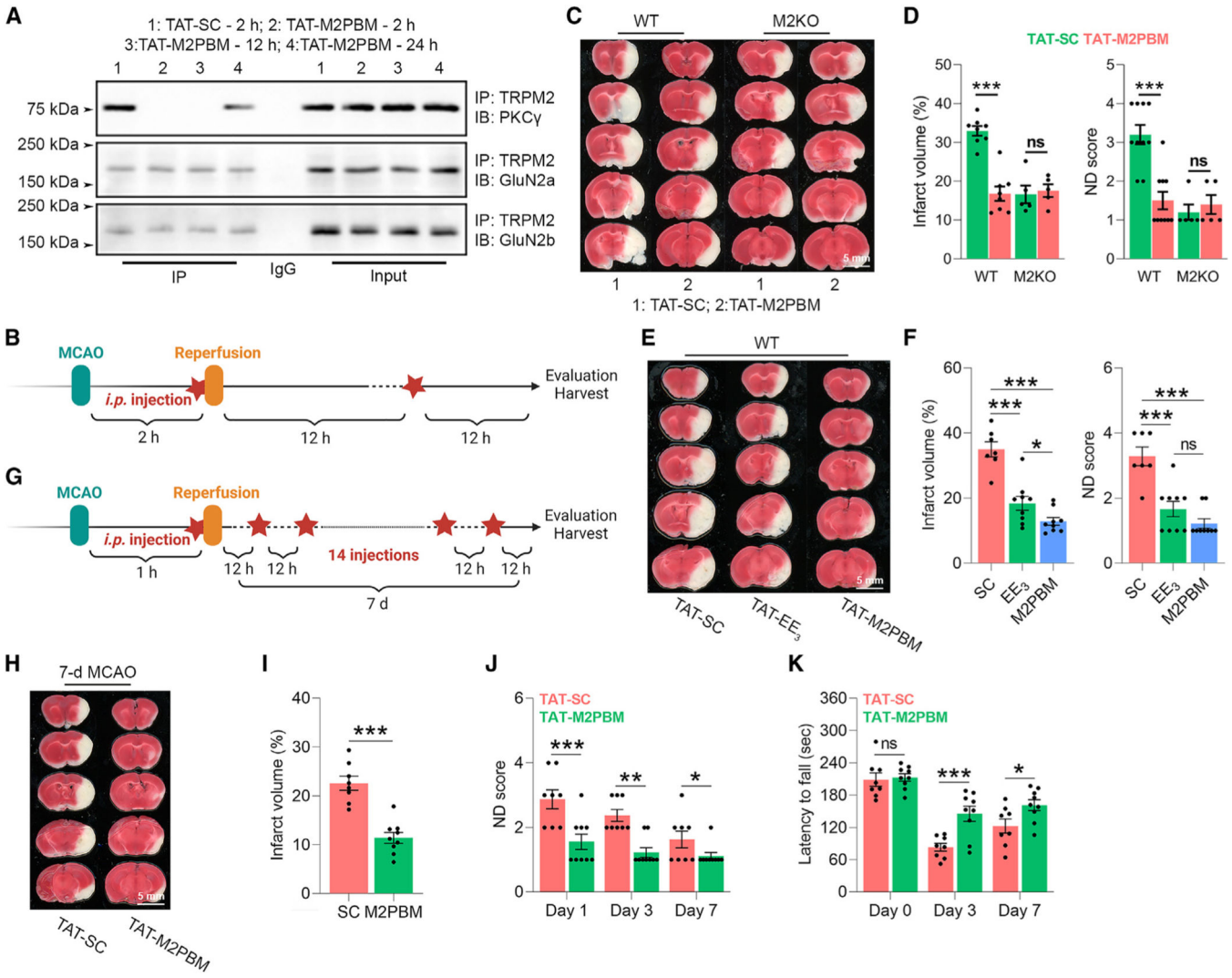

Figure 6. TAT-M2PBM protects mice against ischemic stroke

(A) Co-immunoprecipitation of PKCγ, GluN2a, and GluN2b by TRPM2 in the brain from WT mice 2, 12, and 24 h after injection with TAT-SC (scramble) or TAT-M2PBM at 100 nmol/kg.

(B) Injection strategy for evaluating short-term protective effects.

(C and D) Brain injury in WT and *Trpm2* deletion (M2KO) mice injected with TAT-SC or TAT-M2PBM (100 nmol/kg) 24 h after MCAO (n = 8, 7, 5, 5).

(C) Triphenyl tetrazolium chloride (TTC) staining showing infract area (white).

(D) Quantification of brain infarction and neurological deficit score.

(E and F) Brain injury in WT mice injected with TAT-SC, TAT-EE_3, or TAT-M2PBM 24 h after MCAO (n = 7, 9, 9).

(E) TTC staining showing infract area (white).

(F) Quantification of brain infarction and neurological deficit score.

(G) Injection strategy for evaluating short-term protective effects.

(H–K) Brain injury in WT and M2KO mice injected with TAT-SC or TAT-M2PBM 7 days after MCAO (n = 8, 9).

(H) TTC staining showing infract area (white).

(I and J) Quantification of brain infarction and neurological deficit score.

(K) Quantification of rotarod test.

ns, no statistical significance, *p < 0.05, **p < 0.01, ***p < 0.001; unpaired t test; mean ± SEM; scale bar: 5 mm.

KEY RESOURCES TABLE

REAGENT or RESOURCE	SOURCE	IDENTIFIER
Antibodies		
TRPM2	Novus	NB110–81601; RRID: AB_1147355
GluN2A	Cell Signaling Technology	4205S; RRID: AB_2112295
GluN2B	Cell Signaling Technology	4207S; RRID: AB_1264223
PKC-γ	Cell Signaling Technology	59090S; RRID: AB_2799557
Pan-cadherin	Cell Signaling Technology	4068S; RRID: AB_2158565
GAPDH	Cell Signaling Technology	5174S; RRID: AB_10622025
GST-Tag	Cell Signaling Technology	2622S; RRID: AB_331670
His-Tag	Cell Signaling Technology	12698S; RRID: AB_2744546
Anti-mouse IgG, HRP-linked Antibody	Cell Signaling Technology	7076; RRID: AB_330924
Anti-rabbit IgG, HRP-linked Antibody	Cell Signaling Technology	7074; RRID: AB_2099233
Bacterial and virus strains		
Escherichia coli BL21(DE3) cells	NEB (New England Biolabs)	C2527
Chemicals, peptides, and recombinant proteins		
Tetrazolium chloride	Sigma-Aldrich	T-8877
NMDA	Tocris	0114
AP5	Cayman Chemical	14539
MK-801	Sigma-Aldrich	M107
PMA	Sigma-Aldrich	524400
H2O2	Thermal Fisher Scientific	200745
EGTA	Cayman Chemical	11706
BAPTA-AM	Cayman Chemical	15551
NP40	Thermal Fisher Scientific	28324
Triton™ X-100	Thermal Fisher Scientific	T-9284
Bovine Serum Albumin	Sigma-Aldrich	9048–46-8
isopropyl-D-1-thiogalactopyranoside (IPTG)	Sigma-Aldrich	I5502–10G

REAGENT or RESOURCE	SOURCE	IDENTIFIER
Neurobasal® Medium	Thermal Fisher Scientific	21103–049
Pluronic™ F-127	Thermal Fisher Scientific	P3000MP
Fura2-AM	Thermal Fisher Scientific	F1221
DAF-FM	Thermal Fisher Scientific	D23844
MitoSOX-Red	Thermal Fisher Scientific	M36008
Rhodamine-123	Thermal Fisher Scientific	R302
Proteinase inhibitors	Sigma-Aldrich	539131–10VL
Phosphatase inhibitors	Thermal Fisher Scientific	78428
Protein A/G PLUS-Agarose	Santa Cruz Biotechnology	sc-2003
2x Laemmli Sample Buffer	BIO-RAD	1610737
TAT-SC (sequence: YGRKKRRQRRR VILLKDHTLEYPVF)	GenScript Biotech	N/A
TAT-M2PBM (sequence: YGRKKRRQRRR WGLDVPNLLISVTGGA)	GenScript Biotech	N/A
DpnI	BioLabs	R0176L
Critical commercial assays		
PKCγ Kinase Enzyme System	Promega	V3391
PfuUltra HF	Agilent	600380–51
Pierce™ Rapid Gold BCA Protein Assay Kit	Thermal Fisher Scientific	A53225
Pierce® Cell Surface Protein Isolation Kit	Thermal Fisher Scientific	89881
ProteoExtract™ Native Membrane Protein Extraction Kit	Calbiochem	444810
Experimental models: Cell lines		
HEK293T cells	ATCC	CRL-3216
Experimental models: Organisms/strains		
C57BJ6 mice	JAX	000664
Global TRPM2 knockout mice	Yasuo Mori’s lab at Kyoto University	N/A
Oligonucleotides		

REAGENT or RESOURCE	SOURCE	IDENTIFIER
Primers for mutagenesis and subcloning; see Table S1	This study	N/A
Recombinant DNA		
GluN1A	Luo et al.[40]	Addgene, 17928
GluN2A	Luo et al.[40]	Addgene, 17924
GluN2B	Luo et al.[40]	Addgene, 17925
PKC-γ	Oancea et al.[41]	Addgene, 112266
PKC-γ-DN	Soh et al.[42]	Addgene, 21239
CKAR	Violin et al.[17]	Addgene, 14860
pET15b vector containing a removable TEV protease recognition site	Zong et al.[6] MilliporeSigma	69661–3
pGEX-4T3 vector containing a removable	Zong et al.[6]	V010916
tobacco etch virus (TEV) protease recognition site	NovoPro	
pcDNA4/TO-FLAG-hTRPM2	Sharenberg AM at University of Washington	N/A
Software and algorithms		
Prism 9	Graphpad	https://www.graphpad.com/
Photoshop 2020	Adobe	https://www.adobe.com/
Illustrator 2020	Adobe	https://www.adobe.com/
NIS-Elements	Nikon	N/A
ImageJ	Schneider et al.[43]	https://imagej.net/ij/
Other		
Rotarod	Maze	https://maze.conductscience.com
Avestin EmulsiFlex C3	ATA Scientific Instruments	https://www.atascientific.com.au/products/avestin-emulsiflex-c3
Glutathione Sepharose 4B column	GE Healthcare	Discontinued
Ni^{2+}-nitrilotriacetic acid (NTA) column	GE Healthcare	Discontinued
Amicon stirred ultrafiltration cell unit	EMD Millipore	UFSC40001
CoolSNAP HQ2	Teledyne Photometrics	https://www.photometrics.com
Ultrasonic cleaner	Thermal Fisher Scientific	CPX952136R

REAGENT or RESOURCE	SOURCE	IDENTIFIER
Axopatch 200B amplifier	Molecular Devices	https://www.moleculardevices.com/products/axon-patch-clamp-system/amplifiers